ABSTRACT

Title of Thesis:	A THERMAL MANAGEMENT SOLUTION FOR COMPACT POWER CONVERTERS
	Daniel Ryan Power, Master of Science, 2016
Thesis Directed By:	Professor F. Patrick McCluskey Department of Mechanical Engineering

Regulated Transformer Rectifier Units contain several power electronic boards to facilitate AC to DC power conversion. As these units become smaller, the number of devices on each board increases while their distance from each other decreases, making active cooling essential to maintaining reliable operation. Although it is widely accepted that liquid is a far superior heat transfer medium to air, the latter is still capable of yielding low device operating temperatures with proper heat sink and airflow design. The purpose of this study is to describe the models and methods used to design and build the thermal management system for one of the power electronic boards in a compact, high power regulated transformer rectifier unit. Maximum device temperature, available pressure drop and manufacturability were assessed when selecting the final design for testing. Once constructed, the thermal management system's performance was experimentally verified at three different power levels.

A THERMAL MANAGEMENT SOLUTION FOR COMPACT POWER CONVERTERS

by

Daniel Ryan Power

Thesis submitted to the Faculty of the Graduate School of the
University of Maryland, College Park, in partial fulfillment
of the requirements for the degree of
Master of Science
2016

Advisory Committee:
Professor F. Patrick McCluskey, Chair
Associate Professor Alireza Khaligh
Professor Michael Ohadi

© Copyright by
Daniel Ryan Power
2016

Acknowledgements

First and foremost I'd like to thank Dr. McCluskey for giving me the opportunity to pursue a graduate degree by accepting me into his research group two years ago. His guidance throughout my undergraduate and graduate studies has taught me much about the electronics packaging field and has served to strengthen my knowledge base. I would also like to thank Dr. Ohadi and Professor Khaligh for serving on my advisory committee and for their advice during the last stages of my project.

I want to extend a special thanks to Ayan Mallik and Professor Khaligh in the Department of Electrical and Computer Engineering for designing the power electronic board used in this study and for housing the setup in their lab. I'd also like to thank everyone in the McCluskey research group including Hannes Greve, David Squiller, Ali Moeini, Mike Fish, and Subramani Manoharan for the tremendous amount of help they've provided me with over the last two years. Their knowledge of electronics packaging and thermal management techniques was invaluable throughout the course of my research. I want to thank Mr. Aroom and Giacomo Fornasini in the machine shop for not only showing me how to use all of the machines necessary for the completion of this project, but also for providing me with general manufacturability insight.

I am very lucky to have made some great friends over the course of my undergraduate and graduate career but unfortunately, naming all of them here individually would be too great of a task. Without all of their assistance in the classroom and support outside of it, I would not have been able to complete this challenging chapter in my life. I also want to extend a very special thank you to my girlfriend, Madison, who has been in my life, in

one way or another, during my entire time at CALCE. Her words of advice and unwavering support are something for which I am truly grateful.

I am also indebted to my mom and my brother, Tim, for their continued support. How they've put up with me for this long, I'm not sure, but without them this would not have been possible. I cannot thank them enough for their patience and understanding with my seemingly always busy schedule and sometimes foul mood. Finally, I want to thank my dad, who left us too soon. For almost 21 years he was more than just a father, he was a teacher, a role model and a friend. He not only taught me the importance of hard work, but also of loving what you do; without him I would not be where I am today.

Table of Contents

Acknowledgements .... **ii**

Table of Contents .... **iv**

List of Tables .... **vi**

List of Figures .... **vii**

List of Abbreviations .... **ix**

1 Introduction **1**

1.1 Thermal Management in Electronics 1
1.2 Power Factor Correction Board Components and Function 4
1.3 Research Motivation 7

2 Literature Review **9**

2.1 Existing Regulated Transformer Rectifier Unit Technology 9
2.2 Heat Transfer Fundamentals in Heat Sink Design 10
2.3 Typical Heat Sink Design Process 12
2.4 Heat Sink Manufacturing 15

3 Thermal Modeling **17**

3.1 ANSYS Icepak Description 17
3.2 Model Building Process 18
3.2.1 Component Level 18
3.2.2 Heat Sink Parametrization 21
3.2.3 Problem Constraints and Boundary Conditions 24
3.3 Solving the Model 28
3.3.1 Turbulent Solver 28
3.3.2 Solution Convergence 30
3.3.3 Mesh Control and Independence 32
3.4 Design Selection 34
3.4.1 Post Processing Objects 35
3.4.2 Performance Plots 38
3.4.3 Pressure Drop Consideration 42
3.4.4 Manufacturability Considerations 43
3.4.5 Model 131 45
3.4.6 Thin Fin Modeling 47

4 Experimental Set Up **49**

4.1 Design Modification and Manufacturing 49
4.2 Fan Selection and Modification 50
4.3 Heat Sink Mounting 54
4.4 Temperature Measurement and Testing Results 57
4.5 Experimental Agreement and Variation 59

5 Conclusions, Contributions and Future Work 61
5.1 Conclusions 61
5.2 Contributions 62
5.3 Future Work 63
5.3.1 Unconventional Heat Sink Design Analysis 63
5.3.2 Thermal Management System Design for DC-DC Converter 63
5.3.3 Develop Final Packaging Structure for the RTRU 64
Appendix A Full Thermal Simulation Results 65
Appendix B Performance Plots for 100% and 150% Loads 69
B.1 Base Height and Fin Length Study Results 69
B.2 Fin Width and Number of Fins Study Results 70
References 71

List of Tables

Table 1-1: PFC power device heat dissipation values 6

Table 1-2: PFC power device heat fluxes 6

Table 2-1: Comparison of commercially available RTRUs to this study 10

Table 3-1: Summary of model parameters used in all heat sink simulations 27

Table 3-2: Summary of Model 131 46

Table 4-1: Experimental Results 59

Table A-1: Thermal simulation results part 1 of 4 65

Table A-2: Thermal simulation results part 2 of 4 66

Table A-3: Thermal simulation results part 3 of 4 67

Table A-4: Thermal simulation results part 4 of 4 68

List of Figures

Figure 1-1: Longitudinal fin (left), rectangular pin fin (middle), and circular pin fin (right) 3
Figure 1-2: Heat sink integrated into a standard power package (not to scale) 3
Figure 1-3: Power MOSFET (left) [From 6] and Schottky Diode (right) [From 7] 5
Figure 1-4: Top side (left) and bottom side (right) of PFC board 7
Figure 1-5: Front view of PFC board 7
Figure 2-1: Pictorial representation of heat spreading in a heat sink [From 14] 12
Figure 2-2: Pin fin heat sink array types 14
Figure 3-1: Icepak GUI menus for sizing and placing blocks (left) and defining material and thermal specifications of blocks (right) 19
Figure 3-2: Icepak diode (left) and MOSFET (right) models 20
Figure 3-3: Top view (left) and bottom view (right) of PFC PCB in Icepak 21
Figure 3-4: Front view of PFC board in Icepak 21
Figure 3-5: Icepak menus for sizing heatsinks (left), defining fin structure (middle) and specifying material (right) 22
Figure 3-6: Front view of Icepak heat sink model (left) and isometric view (right) 23
Figure 3-7: Front view of PFC Icepak model with heat sink mounted 23
Figure 3-8: Isometric view of the completed PFC model (PCB shown as transparent) ... 24
Figure 3-9: Air inlet in Icepak models 26
Figure 3-10: Screenshot of solution controls in Icepak 29
Figure 3-11: Residual convergence plot for one of the heat sink models 31
Figure 3-12: Screenshot of die temperature convergence plot for one heat sink design .. 31
Figure 3-13: Isometric view of default mesh slice 32
Figure 3-14: Mesh independence study results 34
Figure 3-15: Normalized solving time for different mesh sizes 34
Figure 3-16: Isometric view of diode temperature contours - 100% Load 36
Figure 3-17: Side view of diode temperature contours - 100% Load 36
Figure 3-18: Heat sink temperature contours - 100% Load 37
Figure 3-19: Device surface temperature contours - 100% Load 37
Figure 3-20: Inlet pressure contours 38

Figure 3-21: Base Height and Fin Length Study Results - 200% Load........................... 39
Figure 3-22: Comparison of base heat spreading in different heat sink designs 40
Figure 3-23: Fin Width and Number of Fins Study Results - 200% Load 41
Figure 3-24: Pressure Drop vs. Maximum Device Temperature - 200% Load 43
Figure 3-25: Fin spacing comparison to standard mill attachment thicknesses............... 45
Figure 3-26: Front view of Model 131 (left) and isometric view (right)......................... 46
Figure 3-27: Thin fin designs added to fin width and number of fins study 47
Figure 3-28: Heat sink weight vs. device operating temperature 48
Figure 4-1: Machined heat sink Model 131 50
Figure 4-2: Axial fan selected for prototype testing 51
Figure 4-3: Fan operating point [From 25] 51
Figure 4-4: System effect in axial fans [From 26] 52
Figure 4-5: Prototype fan duct 53
Figure 4-6: Heat sink with screws in it 54
Figure 4-7: Single thermal pad sheet 55
Figure 4-8: Model 131 mounted to PFC 56
Figure 4-9: PFC experimental setup 56
Figure 4-10: FLIR C2 thermal camera... 57
Figure B-1: Base Height and Fin Length Study Results - 100% Load............................ 69
Figure B-2: Base Height and Fin Length Study Results - 150% Load............................ 69
Figure B-3: Fin Width and Number of Fins Study - 100% Load 70
Figure B-4: Fin Width and Number of Fins Study - 150% Load 70

List of Abbreviations

AC	-	Alternating Current
Al	-	Aluminum
CFD	-	Computational Fluid Dynamics
CFM	-	Cubic Feet per Minute
Cu	-	Copper
DC	-	Direct Current
GUI	-	Graphical User Interface
IC	-	Integrated Circuit
kW	-	Kilowatt
MOSFET	-	Metal Oxide Semiconductor Field Effect Transistor
PCB	-	Printed Circuit Board
PFC	-	Power Factor Correction
RTRU	-	Regulated Transformer Rectifier Unit
SiC	-	Silicon Carbide
TIM	-	Thermal Interface Material
TO	-	Transistor Outline

1 Introduction

The electronics industry is constantly looking for ways to integrate more functionality into smaller enclosures (i.e., place more high powered components closer to each other). In order to do this, more effective thermal management solutions need to do be developed within given problem constraints. The most effective forms of electronics cooling usually involve either single phase liquid or two phase liquid-gas systems. These allow for much higher heat removal rates than conventional air cooling. However, not all applications allow for the use of such complex (and usually expensive) forms of cooling. The focus of this thesis is to design and implement a thermal management solution for a power electronics board subject to high power densities that only employs air cooling.

1.1 Thermal Management in Electronics

When electronic systems run, they typically do not operate at a perfect 100 percent efficiency. As a result, some of the lost power in the system is dissipated as heat from the devices. This heat needs to be removed from the system in order to keep the system operational. Without adequate heat removal technology, device temperatures can increase significantly which can have negative effects on device and consequently system reliability [1]. Higher temperatures decrease carrier mobility, increase the on state resistance of the device and increase the device's susceptibility to different degradation mechanisms including electromigration and intermetallic formations.

Many high power density applications use liquid cold plates to achieve high heat removal rates. Water, for example, has a thermal conductivity value that is roughly 25 times higher than air and a specific heat that is about 4 times that of air. These properties make cooling with water much preferred to air, however, high flow rates and additional

system components such as pumps, pipes and reservoirs are required to obtain this cooling performance [2]. Additional components reduce the overall reliability of the system and high flow rates increase the forces on the pipes in which the fluid is contained, thus increasing the risk of rupture. The size and weight of a liquid cold plate system will vary greatly depending on the type of fluid used, flow rate required, the number of turns in the piping and the device placement [3]. Water's density is nearly 1,000 times that of air, while oil's, another liquid commonly used for electronics cooling, is nearly 800 times that of air. The contribution of the coolant's weight to the weight of the overall cooling system is, therefore, not insignificant. Any liquid pump used would also contribute significantly to the overall weight of the system because of the high flow rates typically used in liquid cooled systems. In applications where a coolant leak would be catastrophic, air cooling methods are preferred to liquid. Additionally, air is more readily available than other coolants meaning the costs incurred from storing and transporting it would be almost nonexistent.

One of the fundamental principles behind air cooling is increasing the surface area of the object from which heat needs to be removed [4]. The most common method for increasing the surface area of a power device package to promote efficient heat removal is the use of a heat sink [5]. Power electronic devices are typically no more than a few square centimeters in area which makes it difficult to remove heat without any sort of extra surface area. The heat sink is traditionally made of a material with a high thermal conductivity such as copper (Cu) or aluminum (Al). Copper's thermal conductivity is roughly 385 W/m-K while aluminum's is in the range of 160 to 200 W/m-K, depending on the alloy [5]. Although copper's conductivity is much higher, its density is more than

three times that of aluminum which can cause problems when weight is an important criterion for the heat sink design. Once the devices are mounted to the heat sink, a fluid (in this case air) is typically flowed over it to assist in removing heat [5].

Traditional heat sinks can come in a variety of fin styles but three examples are: longitudinal fin (also called parallel plate fin or extruded fin), rectangular pin fin and circular pin fin [5]. Each of the styles (pictured in Figure 1-1) possess their own advantages and disadvantages which will be covered in more detail in section 2.3. In a standard power package, the device is mounted to the heat sink with a thermal interface material (TIM) placed in between. The TIM electrically separates the device from the heat sink while maintaining a thermal connection. A pictorial representation of this configuration is shown in Figure 1-2.

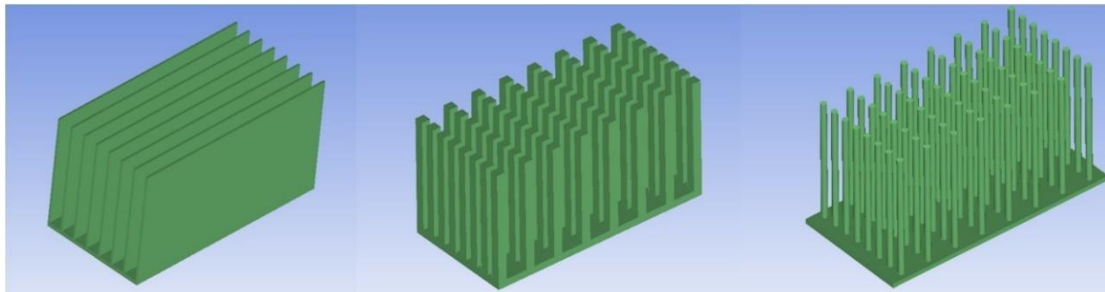

Figure 1-1: Longitudinal fin (left), rectangular pin fin (middle), and circular pin fin (right)

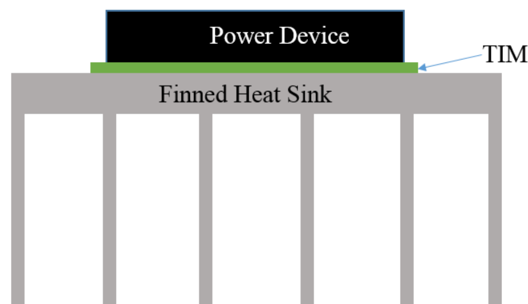

Figure 1-2: Heat sink integrated into a standard power package (not to scale)

1.2 Power Factor Correction Board Components and Function

The Power Factor Correction (PFC) board discussed in this thesis is used as part of a Regulated Transformer Rectifier Unit (RTRU) for alternating current (AC) to direct current (DC) power conversion. The entire RTRU consists of two main power electronic board stages: the Power Factor Correction converter (PFC) and the DC-DC converter (not discussed in this thesis). A three phase 235 volt, AC source at 400 Hz is supplied to the input of the PFC board. The PFC board then converts this to 650 volts, DC which is supplied as the input to the DC-DC converter. The DC-DC converter then finally converts this voltage to 31 volts, DC which is the output of the entire RTRU.

During normal operation it must be able to run at continuously at 160A; this is defined as the 100% loading condition. Every three hours it must be able to run at 240A; this is defined as the 150% loading condition. Additionally, it must be able to operate at 320A periodically; this is defined as the 200% loading condition. Each of these current values can be used to calculate the power of the entire RTRU at each condition by multiplying by the output voltage of 31 volts. That yields power ratings in kilowatts (kW) of: 5 kW for 100%, 7.5 kW for 150%, and 10 kW for 200%. It should be noted that referring to a loading condition as "200%" simply means it is 200% of the nominal loading condition seen by the device, not 200% of the load for which the device is rated. The latter interpretation would indicate these devices are being used at conditions for which they are not suited.

The available board area for the PFC is set from overall RTRU volume restrictions and is set at 7.8 inches by 7.6 inches. The main components of the PFC are six (6) silicon carbide (SiC) power metal oxide semiconductor field effect transistors (MOSFETs) and

six (6) SiC Schottky diodes; both manufactured by Cree Incorporated. These are the devices that dissipate large amounts of heat while the PFC is operating. Pictures of each device from their respective datasheets [6,7] are shown in Figure 1-3.

Figure 1-3: Power MOSFET (left) [From 6] and Schottky Diode (right) [From 7]

There are several other types of devices on the board including DC link capacitors, boost inductors and small integrated circuits (ICs). The ICs on the board include gate drivers, current sensors, current buffers and voltage sensors. However, these devices do not dissipate significant amounts of heat and therefore are considered in thermal simulations only so that their positioning's effect on airflow can be studied. At each of the three loading conditions described at the beginning of this section, the PFC board operates at 98% efficiency or better. The heat loss data for the PFC was provided for each device at each loading condition. Table 1-1 presents a summary of those heat dissipation values.

	Diodes	MOSFETs
100% Load	5.33 W	6.5 W
150% Load	8.0 W	10.733 W
200% Load	10.66 W	15.83 W

Table 1-1: PFC power device heat dissipation values

Heat flux is the standard metric to use when characterizing power density levels for specific applications. The datasheets for the bare die used in both the Schottky diode and power MOSFET give their physical dimensions and are provided on Cree's website [8,9]. Those dimensions along with the values in Table 1-1 were used to calculate the heat fluxes generated by each die and are presented in Table 1-2.

	Diodes	MOSFETs
100% Load	145 W/cm^2	63 W/cm^2
150% Load	217 W/cm^2	103 W/cm^2
200% Load	289 W/cm^2	152 W/cm^2

Table 1-2: PFC power device heat fluxes

The diodes and MOSFETs are positioned on the same side of the board in two separate columns next to each other. The devices are roughly placed in pairs with a few millimeters between each device and then a larger space between each of the pairs. Figure 1-4 shows photographs of the top and bottom side of the PFC circuit board while Figure 1-5 gives a front view. Three of the MOSFETs pictured still have the thermal pads on the back of them so the heat spreader is not visible. The thermal pads will be discussed more in chapters 3 and 4 of this thesis.

Figure 1-4: Top side (left) and bottom side (right) of PFC board

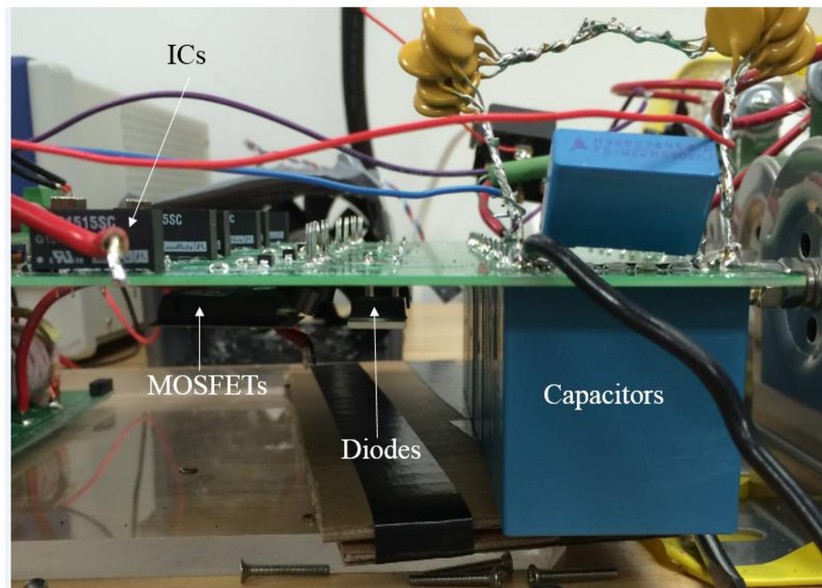

Figure 1-5: Front view of PFC board

1.3 Research Motivation

The increase in demand for more compact power electronic systems means increased cooling capacity will be needed to maintain reliable operation. It is widely accepted that cooling with liquid is preferred to cooling with air because of its higher thermal

conductivity and specific heat values. Liquid cooling, however, requires additional system components and introduces new dangers to the electronics in the system. In systems which are subject to extreme loads, the chances of cooling system components breaking are increased and with that so too are the chances of a coolant leak. Because water, for example, is corrosive and electrically conductive, it could potentially short any device with which it comes in contact. Air cooling methods are easier and less expensive to manufacture and maintain because of the reduction in system components [10]. Air also does not need to be contained as stringently as liquid and possesses the ability to be tied in with the surrounding environment. Air is typically readily available and as long as it can be brought to the appropriate temperature it can be used at almost no additional system cost.

One of the main goals of this study is to show that air cooling is capable of yielding low device operating temperatures when the heat sinks and airflow scheme are designed properly. Throughout the course of this study, the effect of each heat sink geometric parameter (e.g., base height, fin length, fin width, and number of fins) on PFC maximum device temperature will be investigated. As a result, the limits of device temperature rise during operation in this application using conventional air cooling techniques will be explored. The final heat sink design selected for testing will not be based solely on maximum device temperature, however, but also on the required pressure drop and manufacturability.

2 Literature Review

This chapter will begin by describing the current Regulated Transformer Rectifier Unit technologies that exist and their limitations. The next part of the chapter will explore the literature that exists on the design of air cooled heat sinks for certain applications. It will describe the underlying heat transfer principles associated with heat sink design as well as the typical heat sink design process. The last part of this chapter will discuss conventional heat sink manufacturing processes and their limits.

2.1 Existing Regulated Transformer Rectifier Unit Technology

Before beginning the thermal management system design for the PFC board in this study, a literature review of existing RTRU technology was done. This was done to determine which power levels are currently available and what kind of cooling technology is being used. The overall efficiency and weight of the units is also of interest when comparing each unit's performance.

Table 2-1 shows performance metrics of currently available transformer rectifier units as well as the metrics for the RTRU of which the PFC board whose cooling system is being developed in this study is to be a part. The information in Table 2-1 was taken from each manufacturer's website, Crane Aerospace [11] and Avionics Instruments [12], and gives a summary of the available regulated units from each manufacturer. All units described in Table 2-1 use a three phase input. It is clear that an RTRU capable of matching the performance specifications of the unit whose PFC board is being considered in this study, is not yet commercially available. Therefore, a custom thermal analysis for this unit is required. The information on the cooling systems used in the currently available transformer rectifier units was limited to stating that an internal cooling fan is

used. There was no information available on the kinds of heat sinks that are used in the commercially available units.

Manufacturer	Input Voltage (V)	Nominal Output Current (A)	Nominal Output Voltage (V)	Nominal Output Power (kW)	Nominal Efficiency (%)	Weight (lbs.)
Crane Aerospace	115/200	200	28	5.6	85	16
Crane Aerospace	115	250	28	7	87	18
Avionics Instruments	108/118	120	28.5	3.4	85	22
Avionics Instruments	108/118	200	28	5.6	85	22
Avionics Instruments	108/118	400	28	11.2	85	35
This Study	235	160	31	5	95	12

Table 2-1: Comparison of commercially available RTRUs to this study

2.2 Heat Transfer Fundamentals in Heat Sink Design

There are three main modes of heat transfer: conduction, convection and radiation [4]. The primary topic of this thesis is heat sink design which will only involve conduction and convection. Conduction is the transfer of energy in a medium because of the presence of a temperature gradient; it requires physical contact. The standard equation for conduction is known as Fourier's Law:

$$q'' = \frac{q}{A} = k(\frac{dT}{dx}) \tag{2-1}$$

In the conduction equation q represents the amount of heat in the system (W), A is the cross sectional area over which the heat is applied (m^2), k is the thermal conductivity of the material through which the heat travels (W/m-K), T is the temperature (°C), q'' is the heat flux (W/m^2), and x is the position inside the solid (m).

Convection involves the transport of energy through a medium because of the motion of a fluid. The main equation for convection is presented below with h being the convective heat transfer coefficient of the fluid (W/m^2-K), ΔT being the difference in temperature between solid and fluid, and A_s being the total surface area of heat transfer (m^2):

$$q = hA_s\Delta T \tag{2-2}$$

Thermal resistance is used in heat transfer when representing a system as a "circuit," analogous to that used in electronics. Each part of the "circuit" (e.g., device, thermal interface material, heat sink) has a certain thermal resistance value which can be derived using its physical parameters. Thermal resistance is calculated by combining the material's thickness (t), thermal conductivity (k), available heat transfer area (A) and convective coefficient (h) if applicable (i.e., if there is a fluid flowing over the surface of the object). Thermal resistance equations for conduction and convection terms are given below:

$$R_{th_cond} = \frac{t}{kA} \tag{2-3}$$

$$R_{th_conv} = \frac{1}{hA} \tag{2-4}$$

These values are then summed to determine an overall system thermal resistance. The units of thermal resistance are °C/W, therefore it can be used in conjunction with the overall heat dissipation of the object or system to calculate the temperature rise of different parts of the system through this equation:

$$\Delta T = R_{th_sys} \times q \tag{2-5}$$

The heat sources for which heat sinks are designed are typically much smaller in cross sectional area than the base plate of the heat sink. Whenever there is a change in the cross sectional area that is contacting the heat source, heat will start to flow laterally in addition to axially. This phenomenon in a heat sink is shown pictorially in Figure 2-1. When this happens a so called spreading resistance, associated with the lateral movement of heat, is introduced into the system [13]. Closed form mathematical solutions for calculating the spreading resistance in systems exist for the simplest cases (i.e., single source) but when more complex scenarios arise (i.e., multiple sources placed unevenly), the use of a computational model is the recommended method for modeling the spreading behavior. Thermal performance values on datasheets for commercial off the shelf heat sinks rarely account for the additional resistances associated with spreading [14]. This makes a custom thermal analysis for each application imperative to obtaining an accurate heat transfer model.

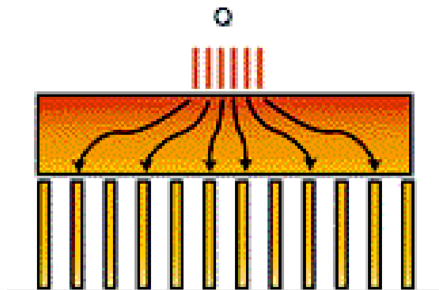

Figure 2-1: Pictorial representation of heat spreading in a heat sink [From 14]

2.3 Typical Heat Sink Design Process

As mentioned in section 1.1, three types of heat sink fin geometries used in electronics are: longitudinal fin, rectangular pin fin and circular pin fin. Before actually designing the heat sink for a specific application, the designer must first decide which geometry he is going to focus on, as trying to design for all three geometries can be very

time consuming. Each of the three geometries possess their own advantages and disadvantages.

Both of the pin fin geometries allow the designer to evaluate staggered arrays in addition to in line arrays. Figure 2-2 shows a bottom view of these two types of arrays for circular pin fins; rectangular pin fin arrays would look similar. For a given fluid velocity, the staggered arrays achieve a higher heat transfer coefficient than the in line and longitudinal fin styles. The staggered arrays remove more heat via convection because the out of line pins serve to disrupt the flow of fluid over the heat sink, which prevents it from developing fully and introduces turbulent eddies to the flow stream, allowing for more heat to be removed by the fluid [15]. This improved thermal performance comes at a cost though: significantly higher pressure drop across the heat sink than the longitudinal fin design.

Higher pressure drop means a larger pump or fan would be required for the system. When there is a pressure drop restriction on the system (i.e., all heat sink geometries must conform to the same pressure standard), longitudinal fin heat sinks actually perform better thermally than pin fin heat sinks [16]. This is in part due to the fact that the longitudinal fin style allows for more surface area within a given volume constraint than either of the pin fin styles. Additionally, while all three heat sink geometries can be manufactured in a variety of methods, longitudinal fins can be machined quicker and cheaper than the pin fin styles.

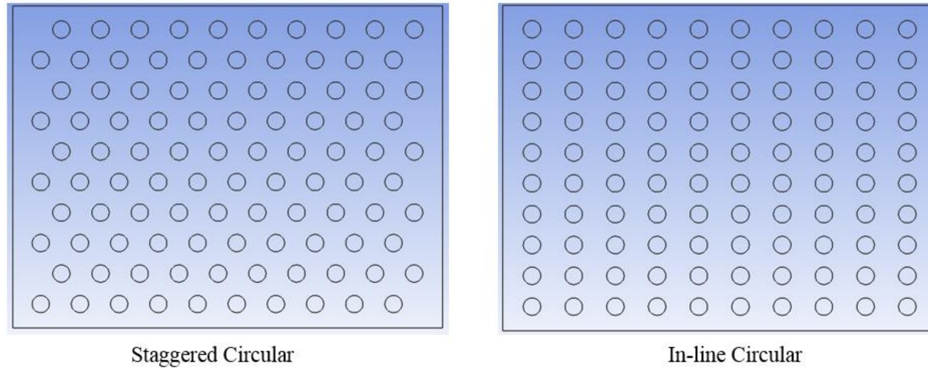

Figure 2-2: Pin fin heat sink array types

Once a designer has decided on a fin geometry, he must decide on the actual size of the various physical parameters of the design. In this study the important design parameters are base height, fin width, fin length, number of fins and consequently fin spacing. Numerous analytical correlations for longitudinal fin geometry under forced convection are presented in [5]. These correlations are useful if either 1) a fixed profile area for the heat sink is known or 2) a given heat dissipation value is known. Unfortunately, these correlations do not provide much insight into what the actual device temperatures would be, which is of interest in this study.

Heat sink design, as is the case with many engineering design problems, is not a problem for which only one suitable solution exists. Instead, multiple designs can achieve the same heat dissipation or temperature distributions. Additionally, more complex designs may only improve performance marginally from an earlier, lower fidelity design. For example, longitudinal fin heat sinks can start to perform worse with an increase in the number of fins [17]. Initially, this may not make sense because one would think that increasing the number of fins increases the surface area which allows for additional heat to be removed from the system. However, eventually the fins become spaced so close

together, that the air ends up flowing around the heat sink instead of through the fin array. This greatly reduces the amount of heat that is removed from the system through convection.

The method described in [18] takes only a single heat source into account when running the thermal simulations but it does provide some general insight into heat sink design. A thicker base will reduce the spreading resistance but will also increase the distance the fins are away from the heat source meaning the heat sink's axial conduction resistance will increase. Additionally, if there is a maximum allowable height for a heat sink design, a thicker base will result in shorter fins which would drive the convective resistance up. Making the base thicker than necessary would also reduce the channel height through which the fluid flows, thus increasing the pressure drop [18].

2.4 Heat Sink Manufacturing

When designing a heat sink for any application it is important to review the manufacturing methods most often used including extrusion, bonding, forging, and machining. Each manufacturing method is limited by the minimum fin thickness and the maximum aspect ratio it can achieve. When discussing manufacturing limits for heat sinks, the aspect ratio is defined as the fin length divided by the space between each fin.

The most common method for producing heat sinks is extrusion. This process involves forcing a solid block of material through a die orifice of the desired cross sectional shape. The maximum aspect ratio that can be achieved through extrusion is approximately 8:1. The minimum fin thickness that can be produced is 1 mm [19].

Bonding is a process in which extruded plates are attached, using a thermosetting thermally conductive epoxy or solder, to a base plate. This allows for much higher aspect

ratios than extruding (about 60:1) but requires special machining for the base plate. The minimum fin thickness for bonding is 0.75 mm [19].

Forging uses a punch to force raw material into a molding die. One issue with this process includes the possibility of material getting caught in the molding die, leading to fins of uneven height. Cold forged heat sinks, however, result in denser and stronger fins than those produced by other processes. The maximum aspect ratio that can be achieved through forging is 50:1 and the minimum fin thickness that can be produced is 0.4 mm [19].

Machining a heat sink involves removing material from a solid block to create the spaces between the fins. This is typically accomplished by using a gang saw or other saw attachment on a milling machine, however, fins can become damaged during the process and often require secondary operations to finish. The maximum aspect ratio that can be achieved through machining is 50:1 and the minimum fin size that can be produced is 0.5 mm [20]. It should be noted that the authors in [20] state that these values for machining are derived and therefore should not be taken as set rules.

3 Thermal Modeling

This chapter will start by giving an overview of the thermal simulation software used to construct the power device and heat sink models for the PFC board. It will then describe how the models were solved, which post processing variables were of interest and the heat sink parameterization process that was used for design purposes. Finally, it will outline the design and manufacturing criteria used to make the final heat sink design selection for testing.

3.1 ANSYS Icepak Description

ANSYS Icepak is a thermal analysis software program geared towards modeling electronic components and systems. The user builds the model of the system in Icepak but the program then uses the computational fluid dynamics (CFD) program ANSYS Fluent to solve it. Icepak allows users to model heat transfer between solids and fluid flow over bodies. It is useful for modeling operating conditions that would be difficult to recreate physically and for taking measurements at places that would be inaccessible in a physical setup [21].

Icepak models are created as a system of blocks over which the user has control of the size, position, material and thermal properties. Icepak has built in macros for typical elements used for heat transfer in electronic systems including fans, blowers, and heat sinks. Once all the blocks in a system are sized and placed, appropriate thermal boundary conditions can be assigned. Icepak allows the user to assign constant or transient heat dissipation values to blocks. It also allows the user to define the ambient conditions of the system. When all of those things have been completed, the user must then mesh and solve the model. The details of meshing and solving will be explained in section 3.3.

3.2 Model Building Process

This section will discuss the specifics of the component and heat sink models that were created. It will then outline the basic heat sink design process that was used when evaluating potential PFC heat sinks. It will also present the problem constraints for the specific power electronic board studied in this thesis.

3.2.1 Component Level

Because Icepak is intended for electronic systems, there are various built in macros that the user can employ to easily create different package types (e.g., plastic ball grid array, dual in-line package). If a specific package is not available with the macros, the user can create his own device model using a series of blocks with specific material properties. The SiC diode studied in this thesis is packaged in a transistor outline (TO) 220 package and the MOSFET is packaged in a TO-247 package. Neither of these configurations are readily available in the Icepak macros, so custom component models were created for the purpose of this analysis.

The major parts of power devices include the die, heat spreader and molding compound. These parts were created individually in Icepak and then combined as an assembly so that the heat flow through each component could be examined. Each block is sized and placed through a graphical user interface (GUI) menu. The user can define how large each dimension of the block is through either a specified start and end point or a specified start point and length. This menu is also where the user defines the material and thermal specifications for the block. Icepak contains an extensive library of predefined materials used in electronics from which the user can select. All material properties used

in this thesis were taken from that library. Two screenshots of the menu used for sizing the block used to model the diode die are pictured in Figure 3-1.

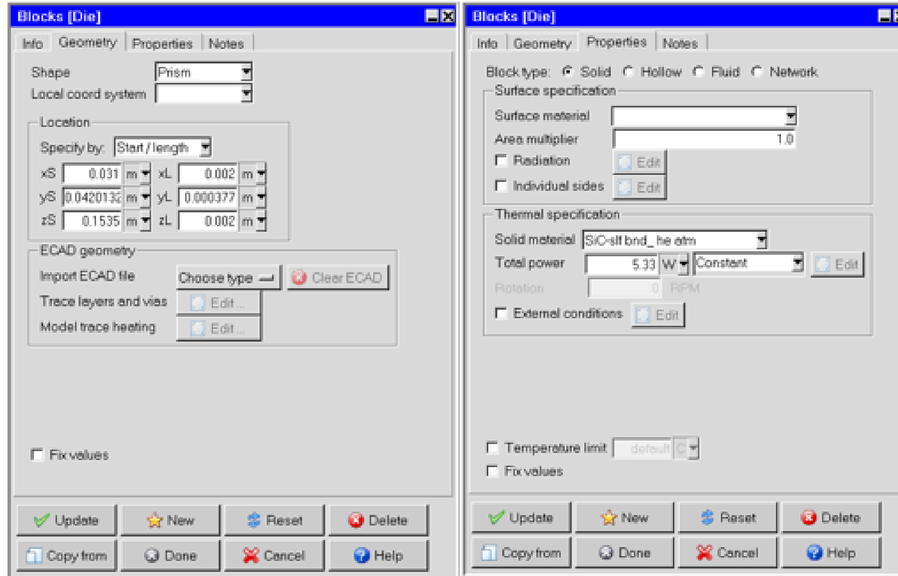

Figure 3-1: Icepak GUI menus for sizing and placing blocks (left) and defining material and thermal specifications of blocks (right)

The die for each of the devices was modeled as a rectangular prism with dimensions taken from the chip datasheets [8] and [9]. The prisms were then assigned silicon carbide as the material and appropriate heat dissipation values from Table 1-1. The heat spreader for each device was modeled in a similar fashion with the dimensions being taken from [6] and [7] and copper being the assigned material. Because of how the die was positioned on the heat spreader, the epoxy molding compound had to be modeled as five separate rectangular prisms. Four smaller prisms were positioned around the die on the same plane. The fifth prism was placed on top of the die and covered the area spanned by the die and the four smaller molding compound blocks. For ease of modeling, the heat spreader on the back of the devices was made so that it covered the entire back of the device, when in reality there is a small amount of molding compound outlining it. The

dimensions of the epoxy molding compound blocks were created such that the overall dimensions of the model device matched that of the datasheets. Icepak models of the diode and MOSFET are shown in Figure 3-2. It should be noted that although the blocks appear transparent in the figures, they are modeled as solid blocks. They are shown to be transparent just so that all parts of the device are visible.

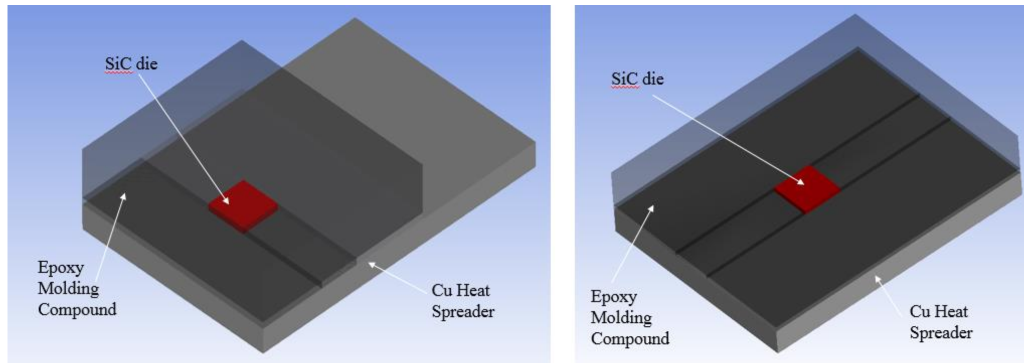

Figure 3-2: Icepak diode (left) and MOSFET (right) models

Although only the diodes and MOSFETs dissipate significant amounts of heat, the entire layout of the board in Figure 1-4 was recreated in ANSYS Icepak. The other devices are included so that their positioning's effect on airflow could be studied. Several different views of the complete PFC Icepak model are shown in Figure 3-3 and Figure 3-4.

Figure 3-3: Top view (left) and bottom view (right) of PFC PCB in Icepak

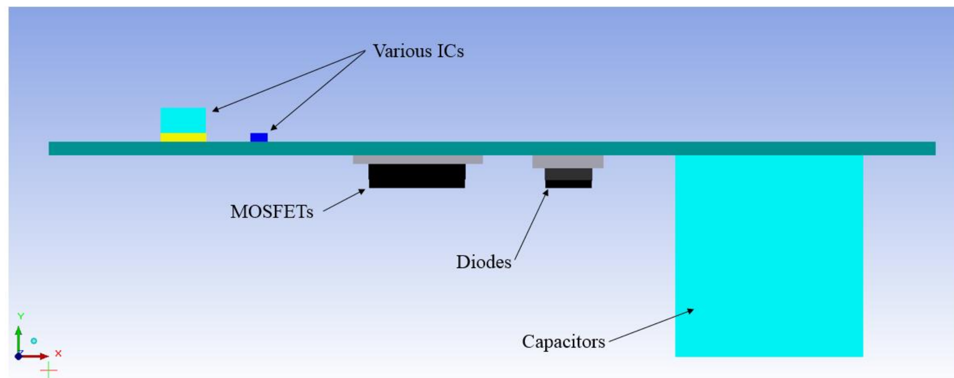

Figure 3-4: Front view of PFC board in Icepak

3.2.2 Heat Sink Parametrization

The longitudinal heat sink fin design (denoted as extruded fin in Icepak) was the one chosen for analysis in this thesis because of the need to minimize pressure drop and its ability to be machined in-house (discussed further in section 3.4.4). The overall size of the heat sink was input in the same fashion as defining the dimensions for the blocks because the heat sink macro uses the same sort of GUI. The heat sink macro has options for defining the fin structure through fin thickness and number of fins, fin thickness and fin spacing or number of fins and fins spacing. The macro also has options for defining

the material of the fins and the base plate. The “default” material is specified at the beginning of the model building process and in this case it is defined as aluminum. Multiple screenshots showing the use of the heat sink macro for one of the heat sink designs analyzed in this thesis are shown in Figure 3-5.

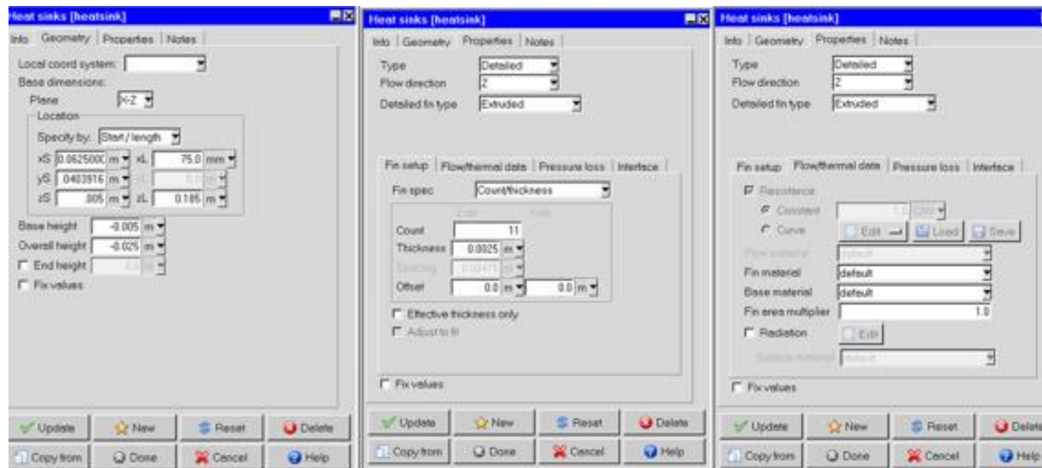

Figure 3-5: Icepak menus for sizing heatsinks (left), defining fin structure (middle) and specifying material (right)

Because of how the power devices were placed, a single heat sink would be attached to the back of all devices. To achieve electrical isolation while maintaining thermal conductivity, thermal pads were placed between the heat sink and the devices. The pads modeled in Icepak were made 0.25 mm thick with a thermal conductivity of 3 W/m-K. These properties were chosen because they matched those of the THERM-A-GAP 579KT gap filler pads which were to be used in the prototype [22]. The purpose of the pads and their properties are discussed in more detail in section 4.3.

The base height, fin length, fin thickness, and number of fins were changed systematically so that the effect of each parameter on the maximum device temperature could be observed. First, a constant fin thickness and number of fins were specified while the base height and length of the fins were varied. The base height and fin length

combination that yielded the lowest device temperature was identified was chosen for the next part of the analysis. The next part of the analysis involved holding the base height and fin length at the values determined in the first part of the study and only varying the number of fins and fin thickness to observe the effect of each of these variables on device temperature. Screenshots of one of the heat sink models in Icepak are shown in Figure 3-6 and the heat sink placement on the PFC is shown in Figure 3-7.

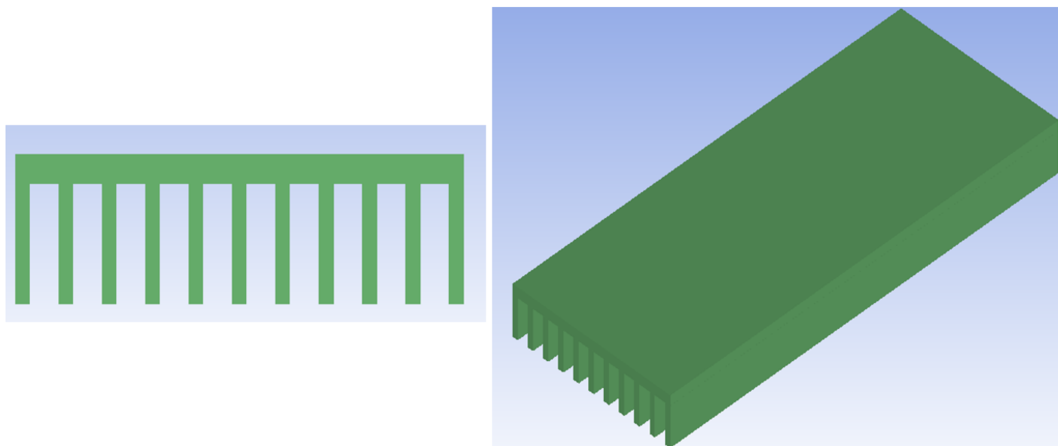

Figure 3-6: Front view of Icepak heat sink model (left) and isometric view (right)

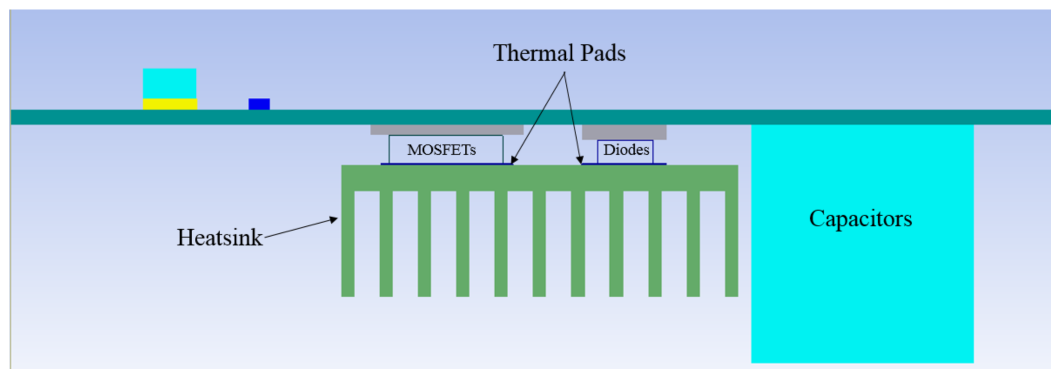

Figure 3-7: Front view of PFC Icepak model with heat sink mounted

An isometric view of the completed PFC Icepak model for one of the heat sink designs is shown in Figure 3-8. The printed circuit board is shown as transparent just so that both sides of the board are visible from the isometric view, however, it is modeled as

a solid block. It should also be noted that the diodes in Figure 3-8 appear to be perfect rectangular prisms simply because that is how Icepak displays assemblies. However, when the model is run, the didoes are modeled as they appear in Figure 3-2.

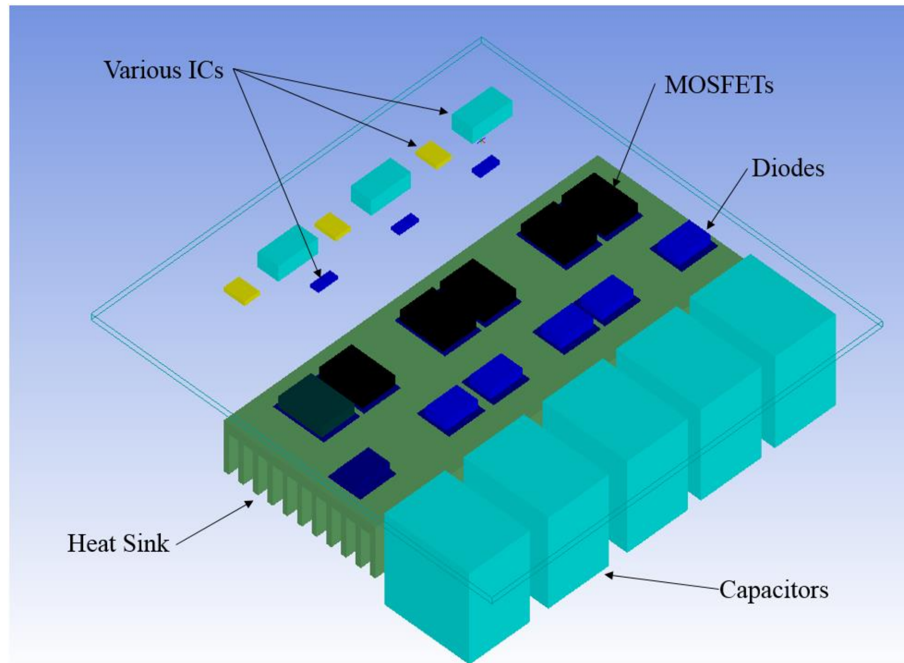

Figure 3-8: Isometric view of the completed PFC model
(PCB shown as transparent)

3.2.3 Problem Constraints and Boundary Conditions

The most obvious constraint in the design process outlined in this thesis is the overall size of the PFC heat sink. The RTRU in which the PFC is to be used is in a system where minimizing weight is crucial. There is an overall weight limit for the RTRU and in order to stay below that the PFC heat sink must not weigh more than 1.6 pounds.

The actual dimensions of the heat sink are limited by the board layout. Because the power devices span the entire length of the board, the heat sink must be 7.8 inches, or about 200 mm, in length so as to accommodate all devices. The DC-DC converter mentioned in section 1.2 must be stacked on top of the PFC board when packaging the

entire unit. Although the DC-DC converter had not yet been fully designed at the time of writing this thesis, the height of the largest components to be included in it was known. That height coupled with the volume restriction placed on the entire RTRU was used to determine the maximum height of the PFC heat sink. Its height may not exceed 1.57 inches, or about 40 mm, but it may be less than that.

The diodes' close proximity to the capacitors places a limitation on how wide the heat sink can extend in that direction. There is no such restriction in the direction of the MOSFETs so theoretically the width of the heat sink could extend all the way to the edge of the circuit board in that direction. However, this would not be preferred because much of the extra heat sink space would likely go unused for heat transfer and therefore only contribute to the weight of the system. To maintain the device placement near the middle of the heat sink and overall balance in the system, its width was limited to 2.95 inches, or about 75 millimeters. Additionally, making the heat sink wider in the direction of the MOSFETs would significantly increase the spreading resistance in the heat sink.

The allowed amount of airflow for cooling in the RTRU is set based on anticipated operating conditions. Overall, no more than 45 cubic feet per minute (CFM) of air can be used to cool the entire unit during operation. This airflow must be appropriately divided between the PFC and the DC-DC converter. Because the DC-DC converter had not yet been fully designed at the time of writing this thesis, 30 CFM was directed to the PFC for the thermal models and experimental testing because of the high heat fluxes in the diodes.

Because the MOSFETs and diodes are the only components dissipating appreciable amounts of heat and because they are concentrated in one area of the board, it would be wasteful to direct airflow over the entire thing. In the actual operating conditions for the

PFC, directing air through only the designated area will be achievable. Therefore, in all thermal simulations of the PFC, air was only directed over the heat sink and the power components. That means that air only flowed through the red rectangle in simulations as shown in Figure 3-9.

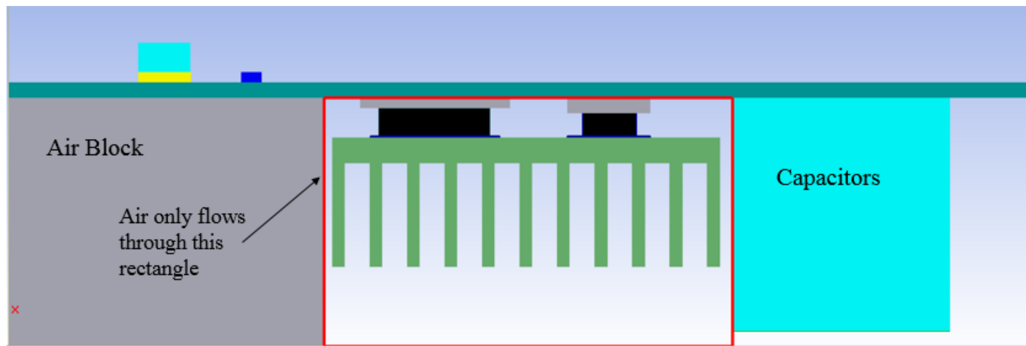

Figure 3-9: Air inlet in Icepak models

An advantage to minimizing the area through which the air flows is that since the volumetric flow rate is fixed, reducing the flow area will increase the air velocity. Increasing the fluid velocity typically means an improvement in thermal performance because it increases the amount of heat the fluid can remove from the system as well as the rate at which it can be removed [23]. To assist in directing the airflow over the heat sink, air blocks were added to the model to maintain the airflow's streamlines in the direction of the heat sink.

In Icepak, the rate of air flow through an opening is specified by fluid velocity instead of volumetric rate. The size of the opening in Figure 3-9 is 79 mm wide by 47.95 mm tall. For a given volumetric flow rate, Q, the fluid's velocity, V, through a certain sized opening, A, can be calculated from:

$$V = \frac{Q}{A} \tag{3-1}$$

All parameters of the problem must be converted to the same unit system. To accomplish this, Q was converted from CFM to cubic meters per second and A was converted from square millimeters to square meters so that the resulting V was in meters per second. For 30 CFM through an opening 79 millimeters by 47.95 millimeters, the resulting air velocity is 3.74 meters per second. The air velocity at an inlet, along with the temperature and pressure at the inlet, can be specified using a GUI similar to those in Figure 3-5. The air temperature at the inlet was specified to be 25 degrees Celsius and the gauge pressure at the outlet was set to 0 Pascals (Pa) so that the pressure drop down the system could be monitored. A summary of all problem parameters constant across all models is shown in Table 3-1.

Maximum Heat Sink Weight	1.6 lbs.
Maximum Heat Sink Height	40 mm
Heat Sink Width	75 mm
Heat Sink Length	200 mm
Inlet Air Temperature	25°C
Inlet Air Flow Rate	30 CFM
Inlet Air Opening Width	79 mm
Inlet Air Opening Height	47.95 mm
Inlet Air Velocity	3.74 m/s
Air Pressure at Outlet (Gauge)	0 Pa

Table 3-1: Summary of model parameters used in all heat sink simulations

3.3 Solving the Model

This section will outline the process by which the thermal simulation models were solved. It will discuss the values monitored during the solving process to ensure solution convergence as well as the mesh independence study that was carried out on the models.

3.3.1 Turbulent Solver

When solving any finite element model with a CFD program such as ANSYS Fluent, the type of fluid flow needs to be identified. Computational solvers use different equations and residual metrics depending on the type of flow in the problem. The Reynolds number (Re) is a metric used to characterize whether a flow is laminar, transitional or turbulent. It is a function of the hydraulic diameter (D_h), the fluid density (ρ), the fluid viscosity (μ) and the fluid velocity (V). The hydraulic diameter depends on the cross sectional area through which fluid is flowing and can generally be calculated as a function of cross sectional area (A) and wetted perimeter (P). For a rectangular cross section, as is the case in this thesis, the wetted perimeter is defined as twice the width (W) of the rectangle plus twice the height (H). Equations for the hydraulic diameter of the airflow inlet and the Reynolds number of the flow:

$$D_h = \frac{4A}{P} = \frac{4HW}{2H+2W} = \frac{2HW}{H+W} \tag{3-2}$$

$$Re = \frac{\rho V D_h}{\mu} \tag{3-3}$$

If the Reynolds number of a flow is below 2300 it is considered laminar. If it is between 2300 and 4000 it is typically considered transitional and if it is over 4000 it is considered turbulent [4]. The hydraulic diameter for the flow over the PFC heat sink was calculated using the “Inlet Air Opening Height” and “Inlet Air Opening Width” values

from Table 3-1 in conjunction with equation 3-2. The velocity of the air is always 3.74 m/s and the density and viscosity of air were taken from Icepak's material library. Combining these values using equation 3-3 yielded a Reynolds number on the order of 14,000 which means the flow falls safely in the turbulent regime.

ANSYS Icepak gives the user numerous options when selecting a turbulent solver. The one chosen for the PFC heat sink analysis was the turbulent two equation solver (also known as the k-epsilon model). This was chosen because it performs well for external flow and requires minimal computational effort while producing good solution convergence. The advanced solution settings menu in Icepak gives the user the option to change the discretization scheme and under relaxation factors for various parts of the solution (e.g., pressure, momentum, temperature). The default settings for these were used with the exception of momentum and temperature. Those were changed from first order upwind to second order upwind to achieve a higher order of accuracy. A screenshot of the solution settings used is shown in Figure 3-10.

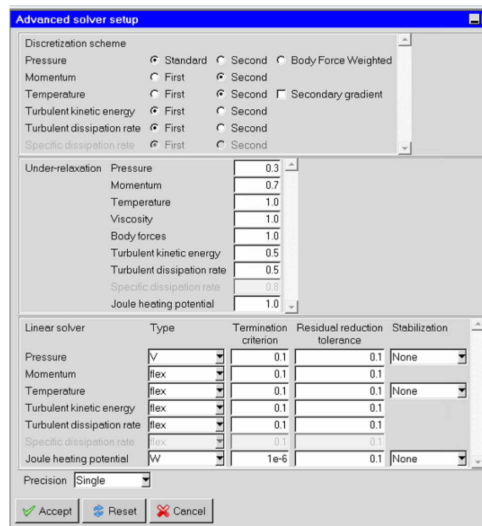

Figure 3-10: Screenshot of solution controls in Icepak

3.3.2 Solution Convergence

The solution process for a CFD problem involves iterating through the appropriate equations multiple times. The solution for each iteration is compared to the one before it and the difference between the two, called the residual, is calculated. Once the residuals for each part of the solution fall below a certain value defined by the user, they are considered to be converged.

In addition to residual convergence, Icepak allows the user to monitor specific parts of the solution while the model is being solved. For example, because the device temperatures were of interest in this study, the MOSFET and diode junction temperatures of the devices furthest away from the air inlet were monitored during the solution process. Once the die temperatures ceased to change with subsequent iterations and the residual values fell below the convergence criteria, the solution was considered converged.

In order to allow the die temperatures to converge, the residual convergence levels for the flow, turbulent dissipation rate, and turbulent kinetic energy were changed from the default 1E-03 to 1E-04 while the level for the energy equation was kept at 1E-07. The number of iterations was changed from the default vale of 100 to 3000 to ensure the solution iterated enough times to achieve convergence. Sample convergence plots for the residuals are shown in Figure 3-11 and converge plots for die temperatures of the worst case diode and MOSFET are shown in Figure 3-12.

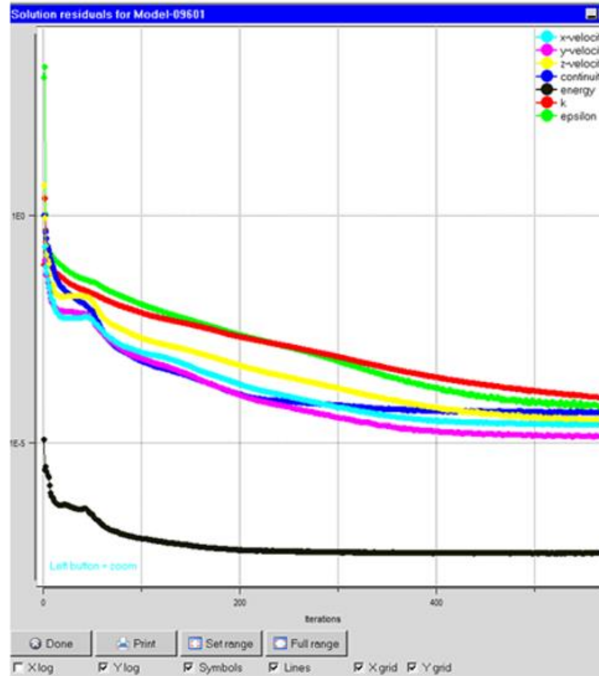

Figure 3-11: Residual convergence plot for one of the heat sink models

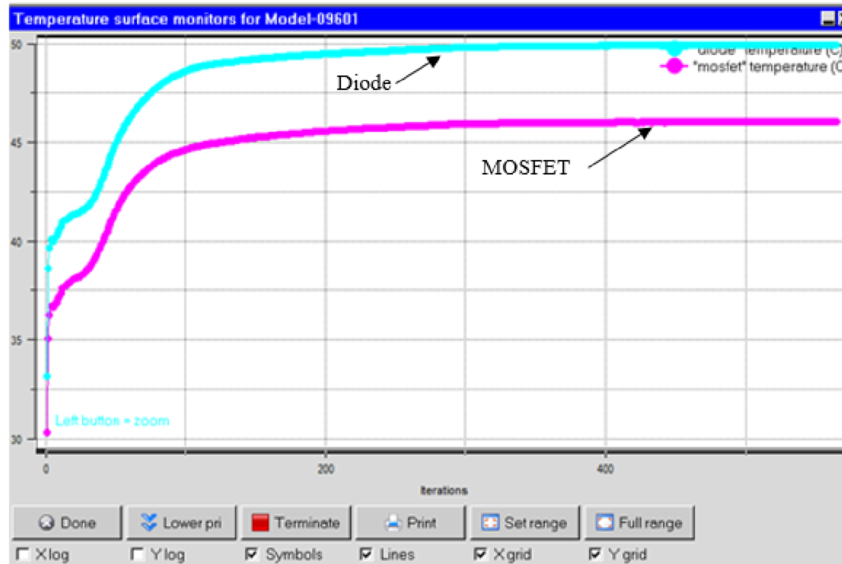

Figure 3-12: Screenshot of die temperature convergence plot for one heat sink design

3.3.3 Mesh Control and Independence

Icepak automatically creates a default mesh size based on cabinet geometry. This default setting produced a mesh with between 600,000 and 800,000 elements for most of the heat sink designs modeled. The mesh can be modified to make it coarser or finer by changing the maximum element size, the minimum gap size and the minimum number of elements in the gap. If a model contains multiple assemblies, as the models used in this thesis do, Icepak allows the user to mesh the assemblies separately.

The default mesh generated by Icepak for one of the heat sink models is shown in Figure 3-13. Because viewing the entire mesh would be visually overwhelming, only a slice of the mesh is presented here. An isometric view is shown so that the location of the slice in addition to the actual mesh can be observed.

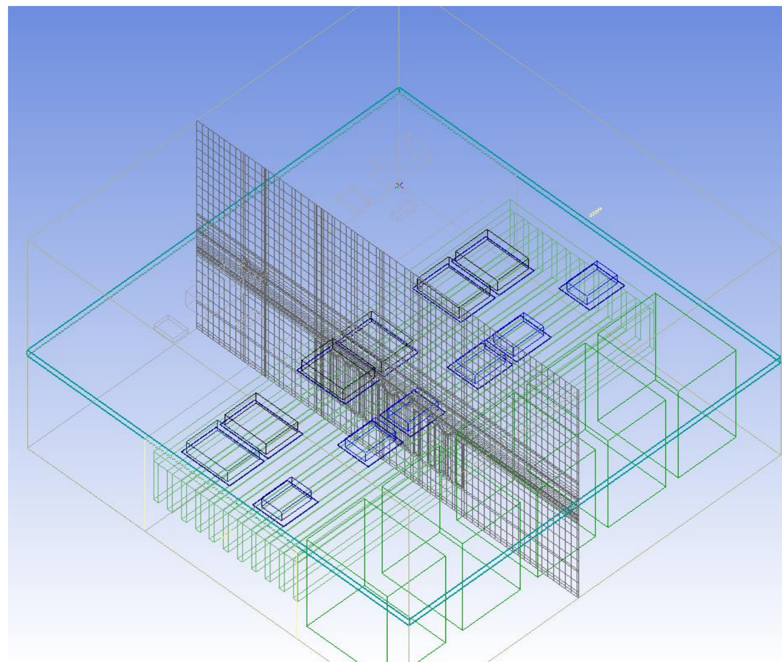

Figure 3-13: Isometric view of default mesh slice

Typically, the finer the mesh, the more accurate the solution, however, a finer mesh also significantly increases the computational power needed. To determine an appropriate number of elements in the mesh, one heat sink model was run seven times, each with a different number of elements to observe how the maximum device temperature changed. Once the number of elements in the mesh no longer significantly changes the maximum device temperature, the solution is considered to be independent of the mesh. The post processing objects in Icepak that were used to analyze model results are discussed in more detail in section 3.4.1.

The results of the mesh independence study are shown in Figure 3-14. The number of elements in the mesh independence study ranged from 480,000 to 3,200,000 and the maximum temperature remained relatively stagnant. The maximum deviation in temperature was less than 1 degree Celsius which corresponds to a 1.6 percent difference in the 200% load case. How the pressure drop of the system changed with mesh size was also studied. While it did fluctuate a bit more than temperature, it still remained relatively stable.

The time to run each of the models was recorded and then normalized with the time it took to run the coarsest mesh (see Figure 3-15). After a point, making the mesh coarser does not save a significant amount of computational time, so a more detailed mesh should be used. Therefore, all subsequent models were run with the default number of elements in order to cut down on the computational effort while maintaining solution accuracy. An iterative approach was taken to design the heat sink meaning a large number of designs were considered. In order to finish the entire analysis in a timely manner, the computational time for each model needed to be reduced.

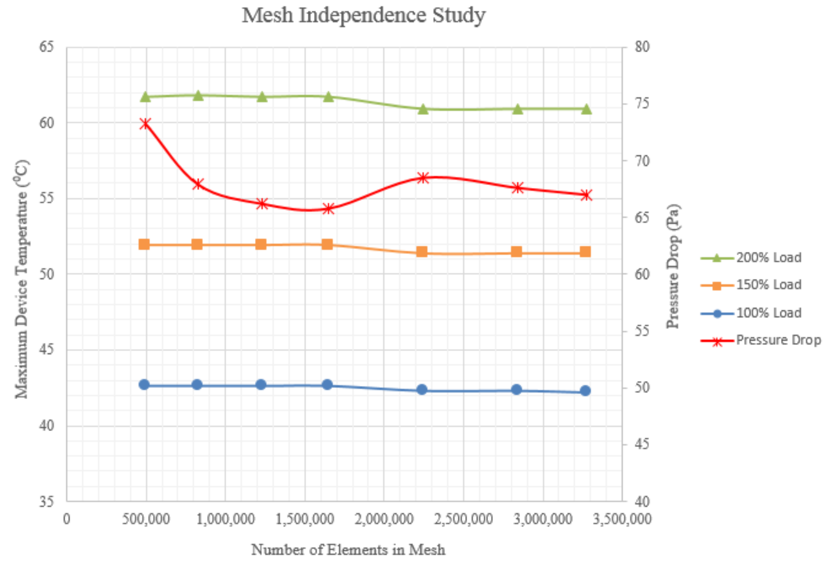

Figure 3-14: Mesh independence study results

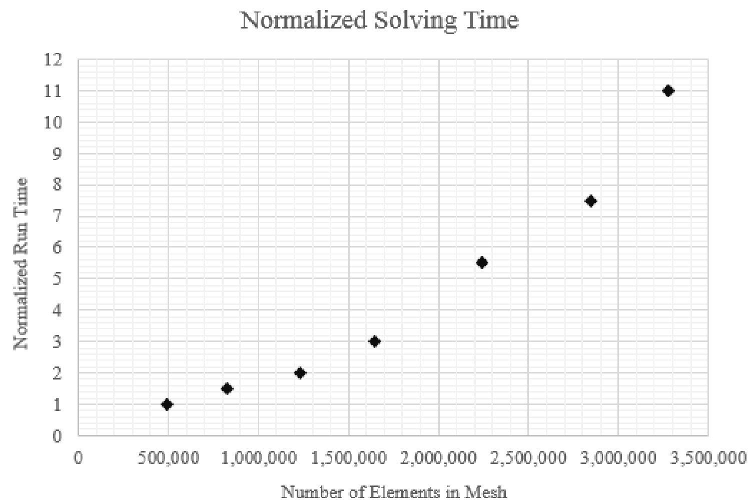

Figure 3-15: Normalized solving time for different mesh sizes

3.4 Design Selection

This section will describe the post processing objects in Icepak that were used to evaluate the performance of each heat sink design. This section will then present the performance plots that were created to compare the heat sink designs that were analyzed.

It will also explain the pressure drop and manufacturability guidelines that were considered when choosing the final design to be used in prototype testing. Finally, it will detail the heat sink design that was selected for use in the PFC prototype.

3.4.1 Post Processing Objects

The main criterion for evaluating the performance of each heat sink design is the maximum junction temperature of the devices. In order to maintain long operating lives of the devices, this temperature was to be minimized. The devices that were furthest away from the air inlet were the ones with the highest junction temperatures. The diode always had a higher predicted junction temperature than the MOSFET because of the smaller die area (i.e., higher heat flux). However, the MOSFET maximum temperatures were typically no more than 5 degrees Celsius lower than that of the diodes.

Icepak allows the user to "cut" through the model and plot contours of various solution metrics on a specified plane. The solution metrics available include temperature, pressure, velocity and displacement among others. These contours are colored to show the different values of whichever metric is selected. An isometric view of one of these cuts for one heat sink design is shown in Figure 3-16 and the side view of that same cut is shown in Figure 3-17.

The side view gives a better look at the outline of each diode and how the temperature contours within each device change down the airflow path. The maximum temperature occurs at the die of the last diode, and for this particular heat sink design it is about 50.8 degrees Celsius. Again, the PCB is shown as transparent so that both sides of the board can be seen. Not all contours for every heat sink design analyzed will be presented in this document, instead a spreadsheet outlining the full results is presented in Appendix A.

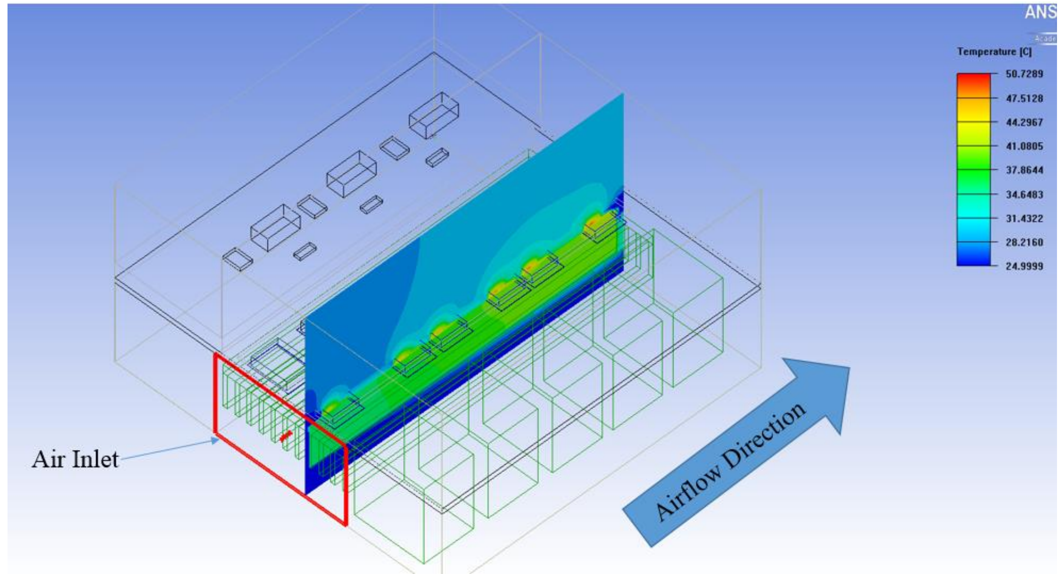

Figure 3-16: Isometric view of diode temperature contours - 100% Load

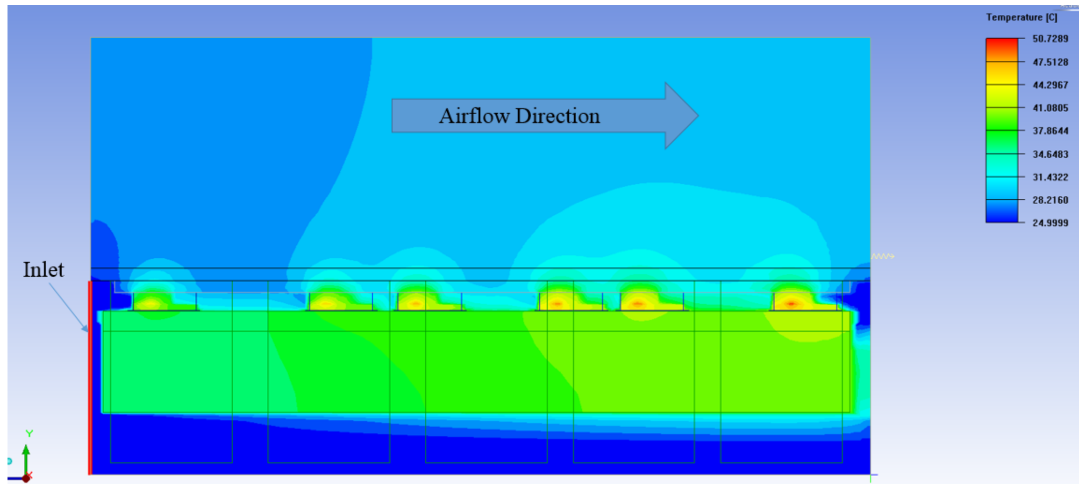

Figure 3-17: Side view of diode temperature contours - 100% Load

In the same way temperature can be plotted for a specified plane, it can also be plotted for a specific object. The temperature distribution in the heat sink was of interest so that heat spreading in the base and fins could be examined. The temperature distribution on the surface of the worst case devices was also of interest because the

temperature on the outer surface of the device is what would eventually be measured to test the performance of the heat sink design selected for testing (explained further in section 4.4). Temperature contours on the heat sink for one of the designs studied are shown in Figure 3-18 and temperature contours on the outer surfaces of the worst case diode and MOSFET are shown in Figure 3-19.

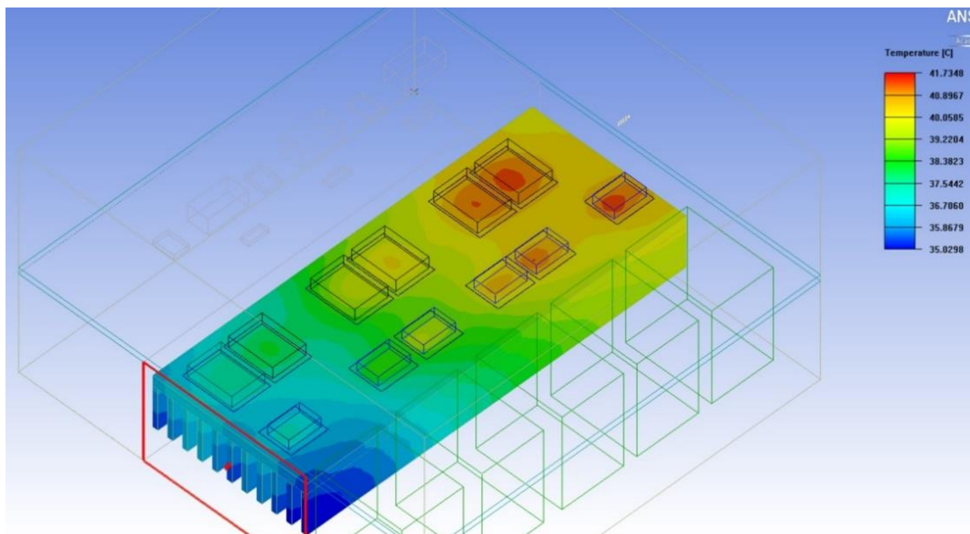

Figure 3-18: Heat sink temperature contours - 100% Load

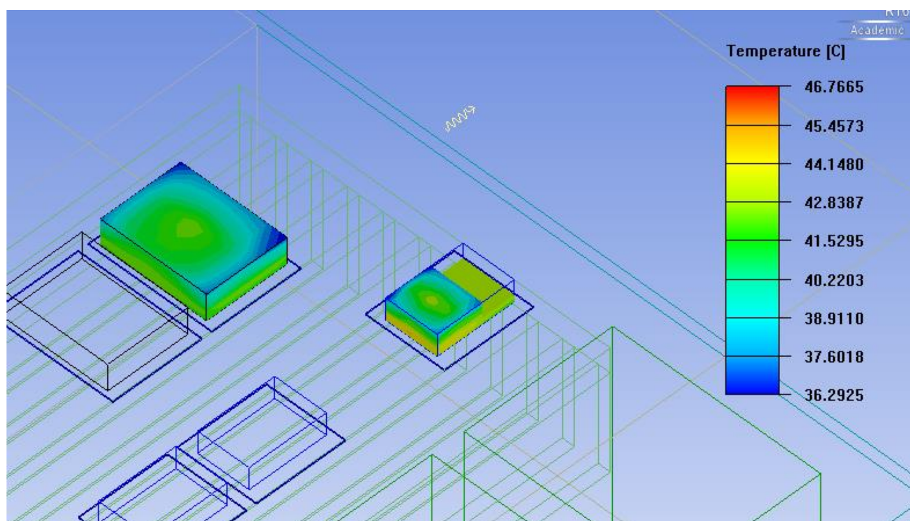

Figure 3-19: Device surface temperature contours - 100% Load

Because the heat sink design eventually selected for the prototype will, in part, be limited by the pressure drop of the available fan, the pressure at the inlet was also checked during post processing. An example cut of the pressure contours at the air inlet is shown in Figure 3-20. The contours in Figure 3-20 show the maximum and minimum pressure at the inlet, however Icepak also returns the area average pressure value which would be of interest when evaluating the total system pressure drop.

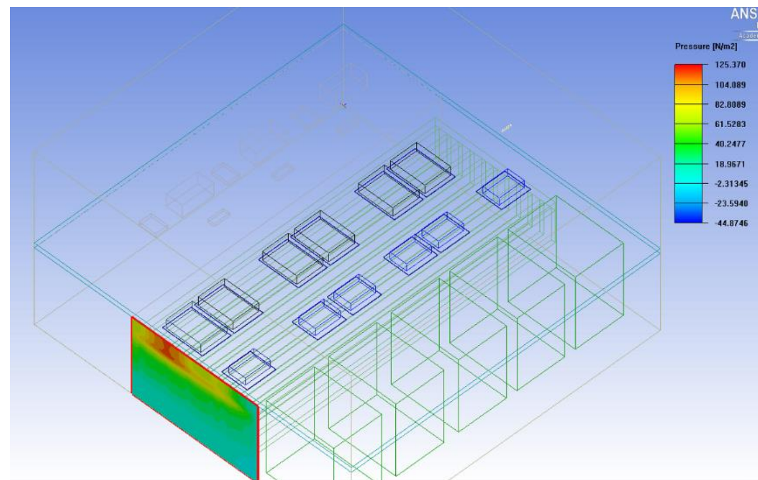

Figure 3-20: Inlet pressure contours

3.4.2 Performance Plots

Although more than just the maximum diode temperature was examined during post processing, it was the metric plotted to compare each heat sink design. As stated in section 3.2.2, first the fin thickness and number of fins on each heat sink design was fixed. Initially, 11 fins, each 2.5 mm wide were modeled because they matched the geometric parameters of a heat sink design readily available for the PFC prototype but whose performance was not yet characterized. The base height and fin length were changed so that the base height and fin length combination that yielded the lowest junction temperature could be identified. The results of this study for the 200% loading

condition are shown in Figure 3-21. The shape of the plots for the 100% and 150% loading conditions is the same, with the only difference being the actual temperatures. Performance plots for those loading conditions can be found in section B.1 in the Appendix B.

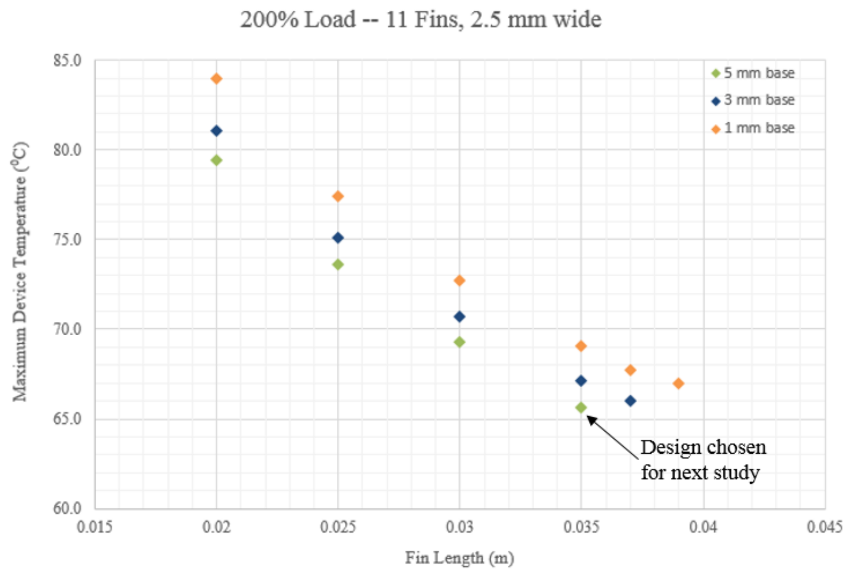

Figure 3-21: Base Height and Fin Length Study Results - 200% Load

As expected, longer fins produced lower maximum device temperatures, however, this was only true to a certain extent. The 1 mm base with 39 mm long fins produced a higher temperature than the 3 mm base with 37 mm long fins which produced a higher device temperature than the 5 mm base and 35 mm long fin combination. This is because when the base is thin, the heat does not spread laterally to all of the fins. Instead, it travels vertically through the base before fully spreading and as a result, parts of the outer fins go unused. This phenomenon at the back end of the heat sink (i.e., the end of the air flow path) in several Icepak models is shown in Figure 3-22. All designs in Figure 3-22 have 25 mm long fins but each has a different base thickness. The green parts of the fins in the

1 mm and 3 mm base designs indicate that the heat from the devices did not fully spread to the edge, thus rendering the outer fins inefficient.

Base heights of 1, 3, and 5 mm were modeled during the first part of the study because it allowed for the full range of fin lengths to be examined without going over the weight limit. A 7 mm base would have made many of the models too heavy but it is shown in Figure 3-22 so that its effect on spreading could be examined. From Figure 3-22 it is clear that increasing the base height to 7 mm does not significantly improve the heat spreading over the 5 mm base and is therefore an unnecessary addition of weight.

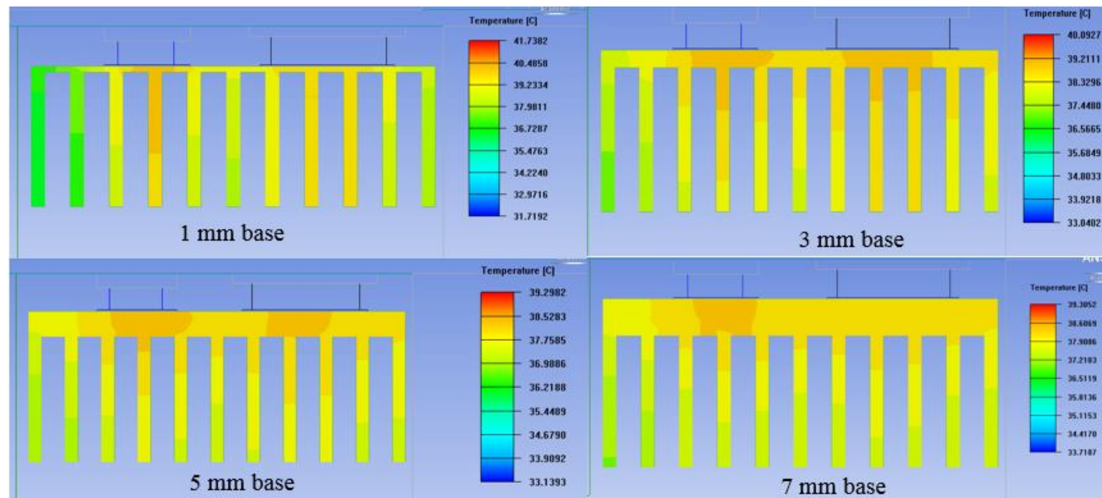

Figure 3-22: Comparison of base heat spreading in different heat sink designs

It is clear from Figure 3-21 that when the overall height is 40 mm, the device temperature is lowest. The 5 mm base and 35 mm long fin combination was then used for next part of the study where the fin width and number of fins were varied. As expected, the more fins there were, the lower the maximum device temperature. After a certain point however, the maximum device temperature no longer decreased significantly despite an increase in the number of fins. The reason for this is likely because when the

space between the fins becomes too small, the air flows around the heat sink instead of through it as discussed in [17]. The results of this part of the study for the 200% loading condition are shown in Figure 3-23. Again, because the shape of the plots for the 100% and 150% loads is the same, those plots are presented in section B.2 of Appendix B.

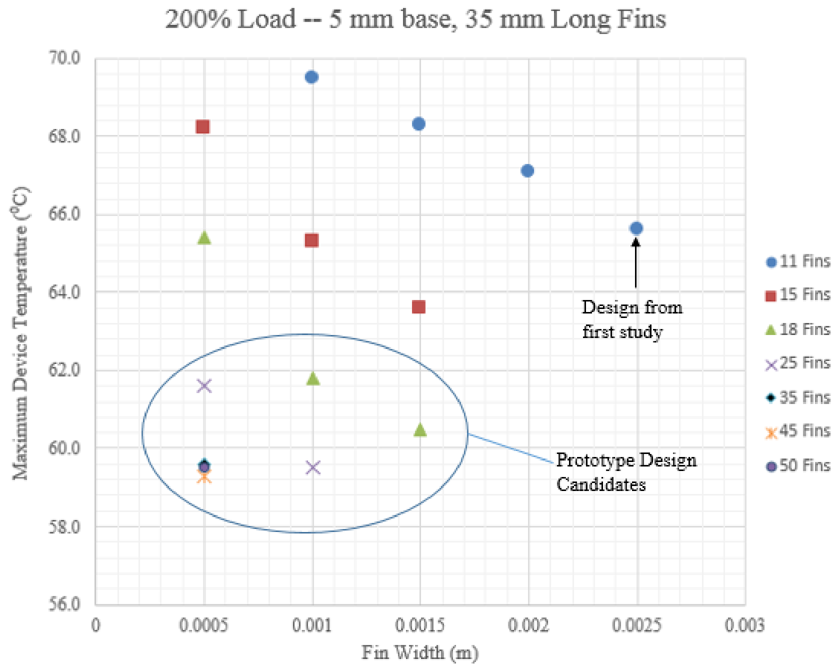

Figure 3-23: Fin Width and Number of Fins Study Results - 200% Load

The plot in Figure 3-23 is useful because it shows several different fin geometries that would achieve similar maximum device temperatures. For example, the plot shows seven different fin geometries that would achieve a maximum junction temperature below 62 degrees Celsius including 18 fins that are 1.5 mm wide, 18 fins that are 1 mm wide and 25 fins that are 1 mm wide. Therefore, other factors such as pressure drop and manufacturability would need to be considered before selecting the final fin geometry for testing.

3.4.3 Pressure Drop Consideration

The fan used to test the PFC prototype will be discussed in more detail in section 4.2. However, for the purpose of completeness in this chapter the pressure drop limit of the fan used is presented. In order to achieve the necessary 30 CFM of air from the fan, the pressure drop down the heat sink must not exceed 0.72 inches of water or about 180 Pa. A plot showing the results from Figure 3-23 against the respective pressure drops of each design and the pressure drop limit for the fan is shown in Figure 3-24. The plot could easily be modified to compare the pressure drops of each heat sink design to a different pressure drop limit. The design selected should fall as far down as possible on the y axis while staying to the left of the pressure drop limit on the x axis.

Although Figure 3-24 only shows the number of fins in each design and not the fin thickness, Figure 3-23 can be used to determine the fin thickness based on the temperature taken from Figure 3-24. Figure 3-24 also shows the device temperature limits in this application using 30 CFM of air with a conventional heat sink fin geometry. Even as the number of fins and pressure drop increase drastically past 35 and 122 respectively, the device temperatures do not continue to fall very far below 60 degrees Celsius. In fact, the temperatures appear to begin slightly increasing after a certain point.

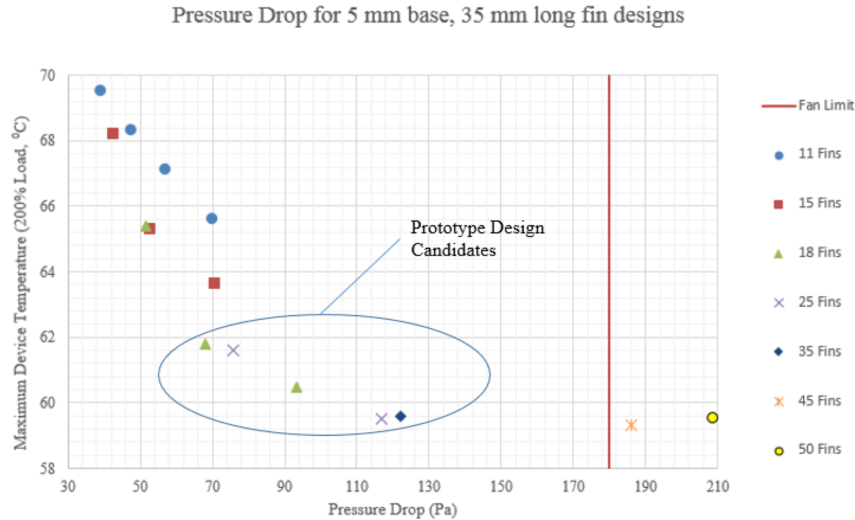

Figure 3-24: Pressure Drop vs. Maximum Device Temperature - 200% Load

3.4.4 Manufacturability Considerations

Limited availability of commercial off the shelf heat sinks and large lead times with most outside heat sink manufacturers led to investigating in-house manufacturing techniques first when evaluating which design should be chosen for testing. Additionally, having an outside company produce the heat sink would have increased the overall cost of the project. The in-house techniques would primarily involve the manual milling machine. Purchasing the needed mill attachment would not only be less expensive than outsourcing the heat sink manufacturing, the attachment could also be used in the future to make additional heat sinks, making in-house milling a cost effective method.

Standard end mills and other milling machine attachments come in prescribed thicknesses or diameters [24]. The entire length of a cut cannot be done in one pass because that would cause the machine to jam from the amount of excess material generated. As a result, multiple passes for each cut would be needed. If the spacing between each of the fins is not the same as or close to that of the standard end mill

thickness, the entire cutting process would need to be performed two or more times. This would lead to an unrealistically long manufacturing time. To avoid this, the final design selected for the PFC prototype was to have a fin spacing either the same as a standard milling machine attachment or close enough such that the effect of changing the spacing to the standard thickness would not significantly affect the predicted thermal performance.

Although the literature review indicated that fins as small as 0.5 mm in thickness could be machined, it was decided that for the PFC heat sink design the fins should be 1 mm or thicker. Attempting to create fins thinner than 1 mm would make them susceptible to warping while making the rest of the cuts. The warping would be a product of the aluminum heating up while being cut and of the vibrations from the milling machine attachment. It should be noted that the reason heat sink designs were modeled with 0.5 mm thick fins was because initially, only the literature was consulted.

Figure 3-25 shows the fin spacing of heat sink designs that fell below the pressure drop limit in Figure 3-24 and had fins with thickness of at least 1 mm. It also shows several standard milling machine attachment thicknesses (indicated by the solid colored lines). The design selected for manufacturing would fall as far down on the y axis as possible while also being on or very near one of the solid colored lines. Again, all designs in Figure 3-25 could be machined, it would just take more than one set of cuts to do them depending on the prescribed fin spacing.

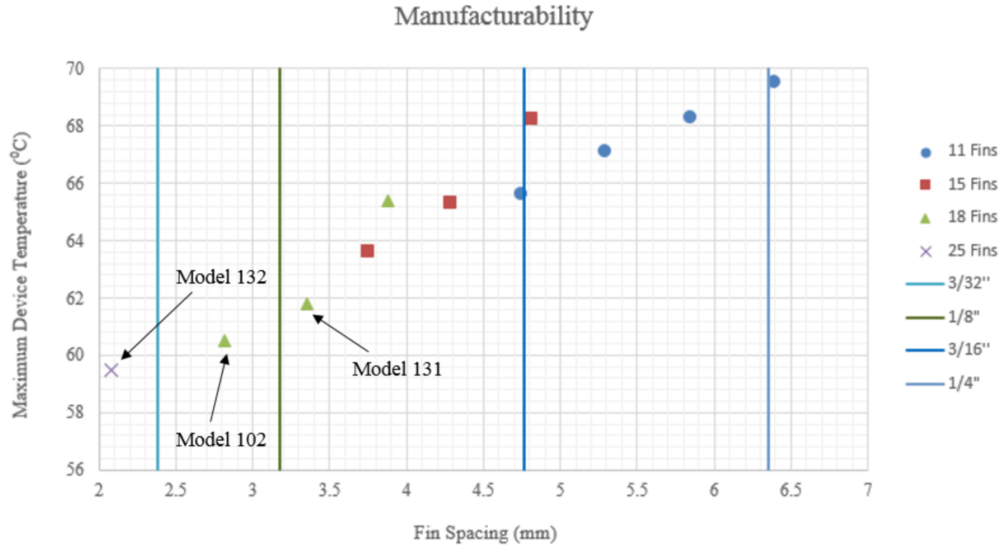

Figure 3-25: Fin spacing comparison to standard mill attachment thicknesses

3.4.5 Model 131

Models 102, 131 and 132 yield low maximum device temperatures and all fall relatively close to a standard milling machine attachment line. Despite the fact that Model 102 and Model 132 produce lower maximum temperatures than Model 131, Model 131 was selected for the PFC prototype. In addition to falling closer to a prescribed milling attachment thickness line, Model 131 also weighed about 0.4 pounds less than Model 102 and 0.3 pounds less than Model 132 (see Appendix A). Table 3-2 outlines the full geometric parameters and predicted maximum device junction temperatures as well as predicted surface temperatures of Model 131 assuming an inlet air temperature of 25 degrees Celsius. The surface temperatures are of interest because that is what will be measured to test the performance of the heat sink design (explained more in section 4.4). Figure 3-26 shows a drawing of heat sink design Model 131 in Icepak.

Geometric Parameters of Model 131							
Overall Width (mm)	75	Overall Length (mm)	200	Overall Height (mm)	40	Fin Spacing (mm)	3.35
Base Height (mm)	5	Fin Width (mm)	1	Number of Fins	18	Heat Sink Weight (lbs.)	1.2
Predicted Device Junction Temperatures with 25°C Air at the Inlet (°C)							
100% Load			150% Load			200% Load	
42.6			51.9			61.8	
Predicted Device Surface Temperatures with 25°C Air at the Inlet (°C)							
100% Load			150% Load			200% Load	
34.1			40.0			45.6	

Table 3-2: Summary of Model 131

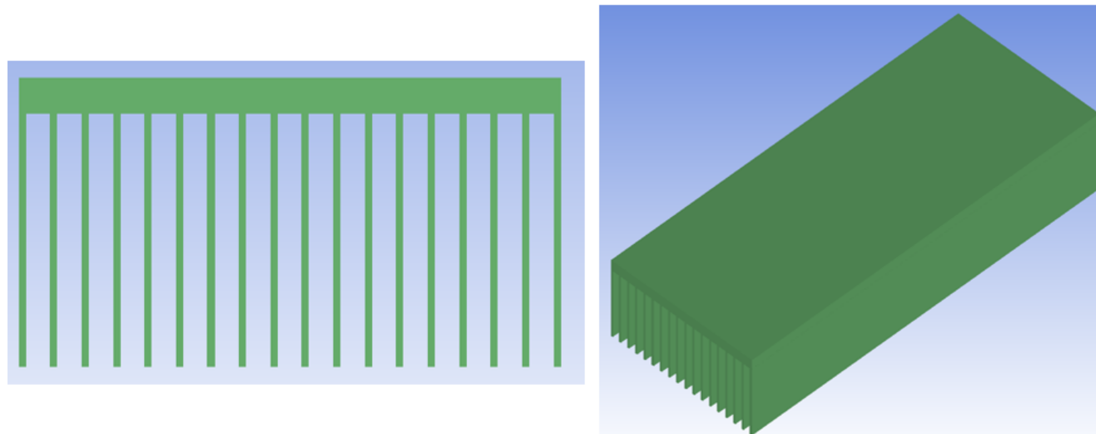

Figure 3-26: Front view of Model 131 (left) and isometric view (right)

3.4.6 Thin Fin Modeling

Several manufacturing constraints needed to be imposed in order to facilitate a timely completion of the heat sink prototype. If these manufacturing considerations were removed, additional designs could be considered. In an effort to reduce weight without sacrificing thermal performance, fins as thin as 0.25 mm could be considered. This section will explore the thermal performance of thin fin heat sink designs at the 200% (10 kW) overload condition and compare it to that of the heat sink designs analyzed in the previous sections. Figure 3-27 shows a continuation of Figure 3-23 with 0.25 mm thick fin designs modeled.

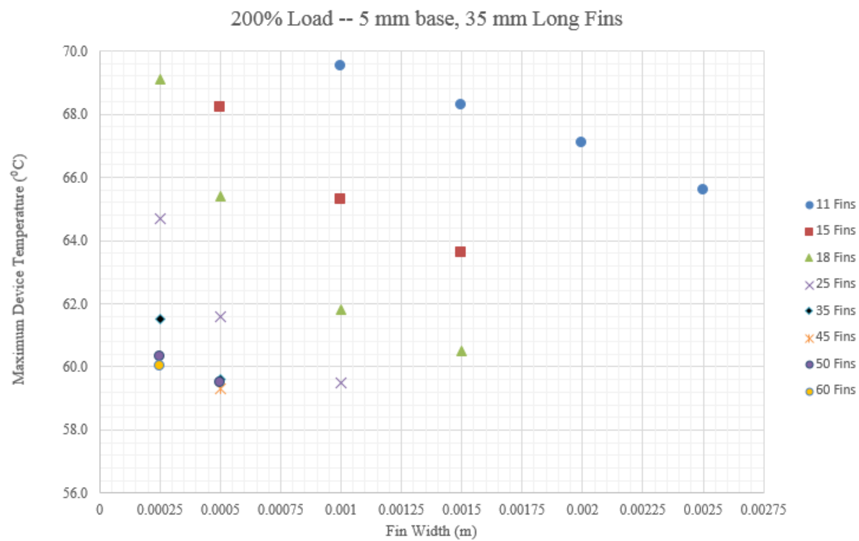

Figure 3-27: Thin fin designs added to fin width and number of fins study

While the predicted maximum device operating temperature does not go down much with the addition of more, thinner fins, the overall weight of the heat sink does go down. Figure 3-28 shows a plot of heat sink weight (organized by fin width) versus predicted maximum device temperature. Comparable thermal performance but an overall lighter

heat sink are achievable with the thinner fins. For example, a heat sink with 0.5 mm wide fins weighing close to 1.5 pounds would bring the maximum device operating temperature down below 60 degrees Celsius. However, a heat sink with 0.25 mm fins would also bring maximum device operating temperatures down near 60 degrees Celsius while weighing less than 1 pound.

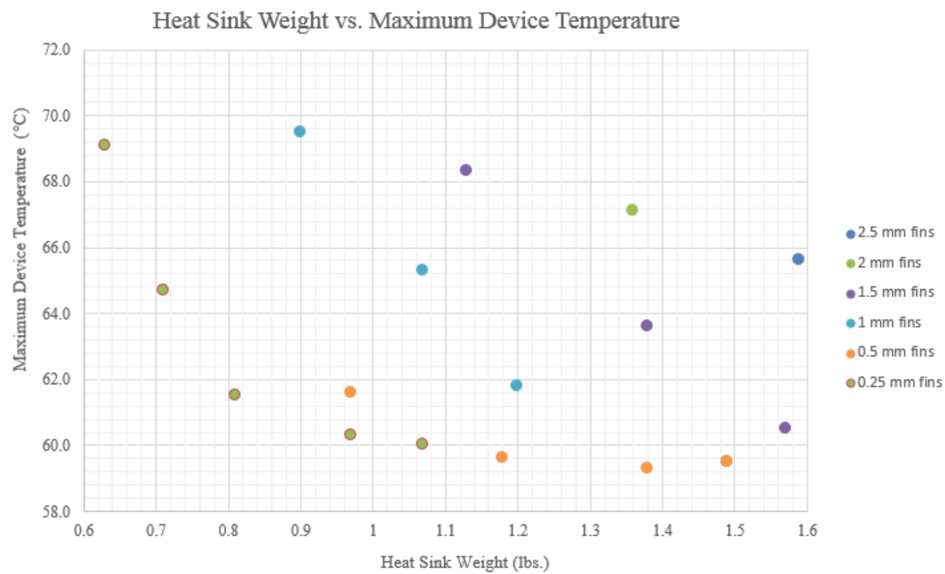

Figure 3-28: Heat sink weight vs. device operating temperature

4 Experimental Set Up

First, this chapter will describe the manufacturing process used to create Model 131. It will then detail the process by which the fan was selected and modified for use in the PFC prototype and describe how the heat sink was mounted to the PFC board. The final part of the chapter will describe the test that was used to determine the performance of Model 131 and present the results of that test.

4.1 Design Modification and Manufacturing

The overall width of Model 131 had to be modified slightly to account for the actual fin spacing (3.175 mm instead of 3.35 mm), but this change had a negligible effect on the predicted thermal performance of the design. Model 131 was then manually machined out of a solid aluminum block using a 6-inch diameter slotting saw attachment on the milling machine. A slotting saw attachment was used because the severity of the vibrations induced when making such deep cuts would likely have snapped a standard ball end mill. Slotting saws also possess the advantage of being able to remove larger amounts of material with each pass than standard ball end mills. Figure 4-1 shows the completed heat sink and it is clear that when comparing Figure 4-1 to Figure 3-26, there is some variability in the fin and channel widths.

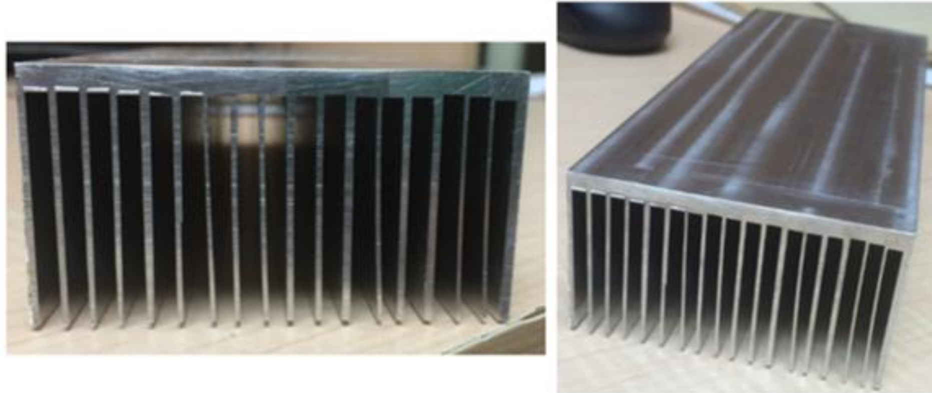

Figure 4-1: Machined heat sink Model 131

4.2 Fan Selection and Modification

In all thermal simulations, a uniform air velocity of 3.74 m/s was used as the inlet airflow condition. When the system is actually running in its intended use environment, producing that flow field will not be an issue, however, because this is a prototype, other methods of air flow needed to be investigated in order to evaluate the performance of heat sink design Model 131.

A DC brushless axial flow fan from Delta Electronics Component Company was selected for use in the prototype test because of its high flow rate capabilities. A photo of the fan is shown in Figure 4-2. The diameter of the fan face is 82.5 mm which means that the entire area through which air would be flowing would be larger than the 79 mm by 47.95 mm area that was specified for airflow in the thermal models (see Figure 3-9). However, because the fan outlet was ducted to the same size as the inlet modeled in Icepak, 30 CFM of air is still required from the fan.

Figure 4-2: Axial fan selected for prototype testing

The point at which this flowrate intersects the fan's pressure versus flowrate curve corresponds to the fan's pressure drop limit in this application. Figure 4-3 shows the fan's curve with the operating point marked as well as the predicted pressure drop for Model 131 [25]. The operating point occurs at about 0.72 inches of water which is roughly 180 Pa while the pressure drop from Model 131 is only about 0.3 inches of water or roughly 70 Pa. This value does not account for additional losses down the duct and the curve is only for operation at 12V. The prototype airflow scheme is covered later in this section.

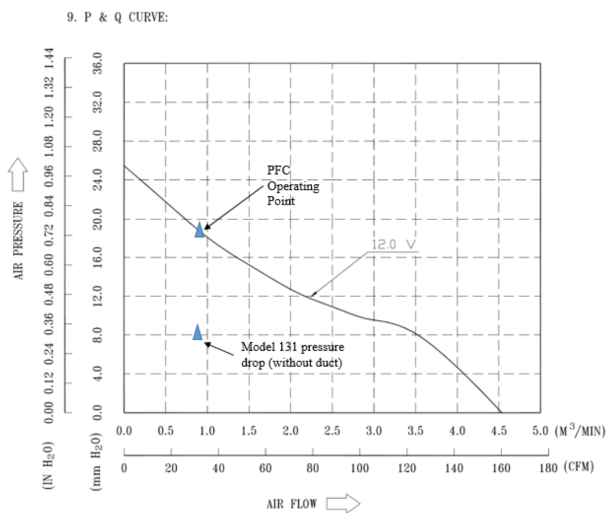

Figure 4-3: Fan operating point [From 25]

Because of the hub in the middle of the axial fan face, the air must first overcome system effect [26]. It is only after the airflow overcomes the system effect that it will

achieve its rated performance as provided by the manufacturer in Figure 4-3. The effective duct length is the minimum duct length needed for the airflow to overcome system effect and fully develop. A picture showing the system effect and effective duct length phenomenon is shown in Figure 4-4.

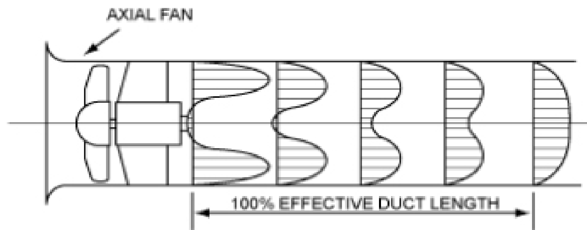

Figure 4-4: System effect in axial fans [From 26]

The effective duct length is calculated based on the maximum output air velocity from the fan [27]. Because the maximum air velocity of the fan during prototype testing is less than 2,500 feet per minute, its effective duct length can be calculated from Equation 4-1. The result is presented in Equation 4-2 and represents the required effective duct length for the prototype:

$$Effective\ Duct\ Length\ (feet) = 2.5\ \times\ Fan\ Diameter\ (ft) \tag{4-1}$$

$$Effective\ Duct\ Length\ =\ .67\ feet = 8.1\ inches \tag{4-2}$$

A duct for the axial fan was constructed out of plywood for several reasons. The first is that it was readily available and provided more structural support than other possible duct materials (e.g., aluminum foil). Plywood can also easily be joined together with wood glue and does not require additional machining expertise to assemble as is the case with sheet metal. The surface roughness of plywood is an order of magnitude greater than that of aluminum foil, but it is still on the order of 10^{-6} m [28]. However, the major losses

down the duct are more strongly correlated with the viscosity of air than the surface roughness of the duct material. The friction factor for turbulent flow down a duct is inversely related to the Reynolds number. The Reynolds number is inversely related to the viscosity of the fluid (in this case air which is on the order of 10^{-5} kilograms per meter second). Therefore, a low viscosity leads to a high Reynolds number which leads to a low friction factor.

The predicted pressure drop for Model 131 is also significantly lower than that which the fan can deliver, therefore the additional losses from the duct did not impede the fan's ability to deliver the required airflow. The initial length of the duct allows the flow from the fan to overcome system effect before transitioning down to the correct inlet size. Additional duct length was added after the transition to allow the flow to overcome the disruption caused by the transition. The duct attached to the fan as well as a front view of the duct outlet are shown in Figure 4-5.

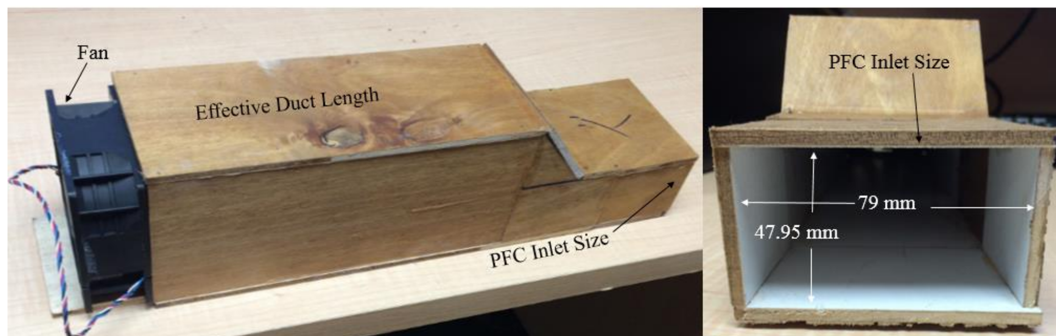

Figure 4-5: Prototype fan duct

The outlet air velocity from the duct was measured with a wind speed anemometer from Kestrel. When placing the hand held device in the air stream, it returns the speed of the air through the top part of it in meters per second. Because the total pressure drop of heat sink Model 131 was considerably lower than the fan's pressure drop limit to achieve

30 CFM, the input voltage to the fan was lowered until the outlet velocity was near the required value to achieve 30 CFM through the system.

4.3 Heat Sink Mounting

Mounting the heat sink to the devices for use in the prototype test set up required threaded holes be inserted into its base plate. These holes were inserted into the locations at which the holes on the devices were located so that screws could be used to maintain contact pressure between the top of the heat sink and bottom of the devices. Standard metal screws were used to attach the MOSFETs because the plastic molding compound covered the entire area with which the screw would be in contact. On the diodes, however, the hole is located on the metal heat spreader so using a metal screw could potentially short the device through the heat sink. Instead, plastic screws were used to attach the diodes. A picture of the heat sink with the screws inserted is shown in Figure 4-6.

Figure 4-6: Heat sink with screws in it

The thermal pads used for the prototype were mentioned in section 3.2.2 and the properties are listed in full on the datasheet [22]. The THERM-A-GAP 579KT pad arrived as a single 4 inch by 4 inch sheet. Twelve separate rectangular pieces

corresponding to the footprint of each device were cut from the single sheet so that they could be placed between each device and the heat sink. The purpose of the thermal pads is to maintain thermal conductivity between the devices and the heat sink while electrically separating them. The THERM-A-GAP 579KT pads have a dielectric strength of 8000 volts per mm, which for a thickness of 0.25 mm should give a dielectric strength of 2000 volts. The maximum voltage any device in the PFC should need to withstand is only 650 volts.

A picture of the single thermal pad sheet is shown in Figure 4-7. Once the thermal pads were cut down to size, the screws could be inserted in the devices to maintain contact pressure between the devices and heat sink while the ducted fan was placed at one end of the PFC board setup. A frontal view of Model 131 mounted to the PFC board is shown in Figure 4-8 and a view of the entire setup is shown in Figure 4-9.

Figure 4-7: Single thermal pad sheet

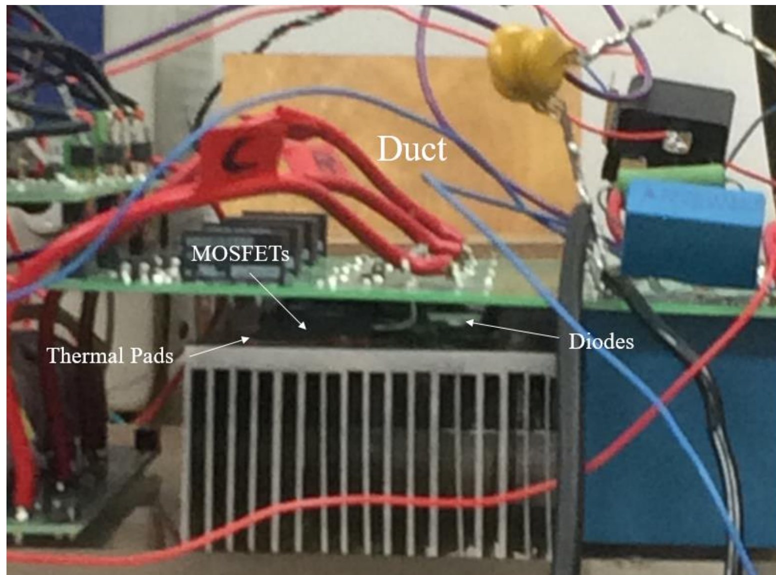

Figure 4-8: Model 131 mounted to PFC

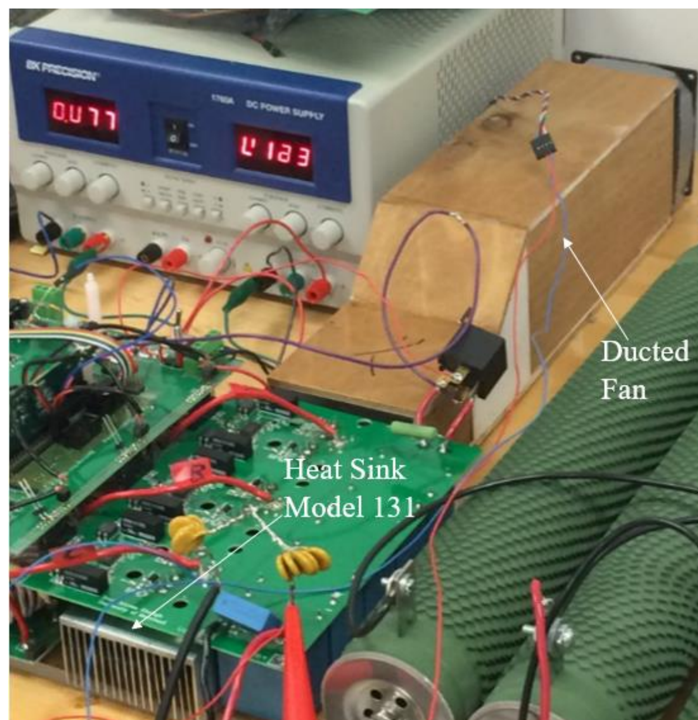

Figure 4-9: PFC experimental setup

4.4 Temperature Measurement and Testing Results

The PFC board was run for 15 minutes at the 100%, 150% and 200% loading conditions. This was done to establish a steady state device temperature at each loading condition. A FLIR C2 thermal camera was used to record the surface temperatures of the worst case devices during operation. This pocket sized device (see Figure 4-10) allows the user to get a thermal map of the objects in the camera's field of view without the need for additional software. The camera automatically adjusts for the highest and lowest temperatures in the field of view so that the entire temperature spectrum in the field can be seen. It also has a rated accuracy of plus or minus 2 degrees Celsius.

Figure 4-10: FLIR C2 thermal camera

Each material's ability to emit energy as thermal radiation is characterized by its emissivity value. The closer this value is to 1, the more efficient a material is at emitting thermal radiation. For example, aluminum has an emissivity value of about 0.1 because most of the light that hits it is reflected and consequently it does not emit as much energy in the form of thermal radiation. Because of that phenomenon, low emissivity materials can prove problematic when attempting to take temperature readings. Most organic and painted materials (such as epoxy molding compound), however, have an emissivity value

close to 0.95. The FLIR C2 doesn't possess the capability for the user to enter an exact emissivity value for an object but does allow for selecting an emissivity category for the objects being examined. The categories are matte (emissivity of 0.95), semi-matte (emissivity of 0.80), and semi-glossy (0.60) which gives the user a range of surface finishes from which to choose.

The ambient air temperature should not be included when comparing predicted to experimental results. Instead, the temperature rise on the surface of the device should be examined. Table 4-1 presents the predicted surface temperature rises of the PFC during operation (along with the corresponding predicted junction temperature rises), the experimental surface temperature rises and the percent error of the temperature rise at each condition. The predicted surface temperature rises were recorded by examining the post processing objects presented in Figure 3-19 and subtracting the ambient air temperature. It should be noted the exact objects in Figure 3-19 are not for Model 131, rather they are for one of the other heat sink designs analyzed and are shown for representative purposes only.

The experimental surface temperature rises of the devices were measured in the gap between the circuit board and heat sink at the end of the airflow path (see Figure 4-8). Because there was a limited amount of space on the actual device for temperature measurement, only the worst case device was examined and spot readings were taken instead of full thermal images. The percent error was calculated using Equation 4-3 with "Ideal" corresponding to the predicted surface temperature rise and "Actual" corresponding to the experimental surface temperature rises.

$$\%\,Error = \frac{Ideal - Actual}{Ideal} \times 100\% \tag{4-3}$$

	Predicted Junction Temperature Rise (°C)	Predicted Surface Temperature Rise (°C)	Experimental Surface Temperature Rise (°C)	Surface Temperature Rise % Error
Model 131-100% Load	17.6	9.1	7.0	23.1
Model 131-150% Load	26.9	15.0	12.0	20.0
Model 131-200% Load	36.8	20.6	16.0	22.3

Table 4-1: Experimental Results

4.5 Experimental Agreement and Variation

All heat sink designs were modeled with the calculated power loss data for each device at each loading condition. These numbers were calculated based on certain device characteristics such as switching frequency, turn on time, turn off time, on state voltage, etc. There is an amount of uncertainty associated with each of these values so when they are combined there is also going to be some uncertainty in the resulting values. As a result, even the most detailed component model will still have some amount of error associated with it.

All of the predicted surface temperature rises ended up being higher than the experimental temperatures. A possible reason for this is because the experimental temperatures were measured with the board open to the ambient air condition while the models were run in an enclosed structure. Having the devices open to the ambient environment during testing would allow for additional heat removal from via natural convection that would have been absent in the thermal models. Additionally, the models included spacers between the top of the device and bottom side of the circuit board (see Figure 3-7), whereas in the experiment, this spacer was absent. The absence of the spacer

would have allowed for more air to flow over the top side of the devices, thus removing additional heat from the system and reducing the experimental temperature rise.

Finally, the uncertainty associated with the emissivity values likely accounted for some of the discrepancies between model and experimental results. Without knowing exact emissivity values of the objects from which temperature readings were being taken or the ability to calibrate the thermal camera with those actual values, there will always be some uncertainty in the experimental results. The rated accuracy of the thermal camera is also something to consider when comparing the experimental results to the model results.

5 Conclusions, Contributions and Future Work

The goal of this research was to design and implement an air cooled thermal management system for a high power converter application. The main result of this study was an air cooled heat sink design for a given power electronic board that allowed for low device temperatures at long term use during nominal and overload conditions. The method described in this study examined the effect of each heat sink parameter on maximum device temperature. Other factors besides maximum device temperature that influenced the design selection were available pressure drop and more importantly manufacturability. The process through which the heat sink prototype was tested was presented and despite slight variability in the machined heat sink, it achieved experimental performance close to that which was predicted.

5.1 Conclusions

To demonstrate the predicted thermal performance, the selected heat sink design was machined and then attached to the PFC board. The experimentally measured surface temperature rises at three different loading conditions were lower than the predicted values with a maximum error of about 23 percent. This discrepancy between model and experimental results is likely a result of uncertainty in the heat loss values and the absence of an enclosure in the experiment.

Although air is a much poorer conductor of heat than liquid, it is still capable of yielding low device operating temperatures through appropriate heat sink and airflow design. The base plate of the heat sink should be thick enough to allow the heat to spread laterally to all fins but not so thick where its improvement to the lateral heat spreading is negligible and therefore its main contribution to the system is unnecessary weight.

Additionally, the width of each fin and the number of fins in the heat sink should be designated such that the air continues to flow through the fin array instead of around the heat sink. The size, number, and location of devices (i.e., heat sources) on the heat sink play a large role in determining appropriate values for each geometric parameter of the heat sink. If an axial fan is used in prototype testing to achieve the desired airflow, appropriate ducting should be utilized so that the air has enough distance to overcome the system effect and so that the air velocity at the outlet is consistent with that in the thermal models.

Using the milling machine to manually create the spaces between the fins is an effective custom heat sink manufacturing method if cost and time need to be minimized. However, in practice, the limit of which fin thicknesses and aspect ratios can be achieved with manual machining differ slightly from those presented in literature.

5.2 Contributions

The results of this study added a number of contributions to the field of thermal management in power electronics as described below:

- Demonstrated the applicability of conventional air cooling techniques in high power systems.
- Developed an approach for reducing electronic component complexity in thermal simulations while producing dependable results.
- Demonstrated the importance of modeling power device configurations in their entirety when designing thermal management systems.

5.3 Future Work

This section describes several areas on which future work could be done to build upon the work presented in this study. These suggestions were developed based on the challenges encountered during the course of this study and the required next steps for fully developing the RTRU.

5.3.1 Unconventional Heat Sink Design Analysis

The results of this study gave a good indication as to what the device operating temperature limits were in this application with a longitudinal fin heat sink. Because the parameter space that could have been explored was so massive, some limits had to be imposed. Without some of those limits, there would be room for more flexibility in the design. Exploring fin width and number of fin combinations with a different base height and fin length than what were used in this study would likely yield a different final design. Combining longitudinal and pin fin styles into one design would introduce a different type of airflow in the heat sink and would change the thermal performance. Using two or more different materials for the base plate and fins of the heat sink may also help improve the thermal performance and drive the maximum device operating temperature down in this application.

5.3.2 Thermal Management System Design for DC-DC Converter

As stated in the introduction chapter, the PFC board is one of two main power electronic boards in a Regulated Transformer Rectifier Unit. The DC-DC converter is the next stage of the RTRU and its board layout differs significantly from that of the PFC meaning the size and weight restrictions of the thermal management system will also differ. The presence of primary and secondary side devices on the DC-DC stage will

introduce unique challenges to the thermal management system design process. The steps used in this thesis can be applied to the DC-DC heat sink design, but the end results will be different.

5.3.3 Develop Final Packaging Structure for the RTRU

This work mainly focused on developing the thermal management system for the front end of a regulated transformer rectifier unit. In order for the final prototype to be implemented, all stages of the converter with their respective thermal management systems need to be integrated. In its actual use condition, the RTRU will not utilize an axial fan to produce the needed air flow, instead air will be provided from the use environment. This means that any enclosure designed for the unit should have appropriately sized vents at the prescribed locations. When finally integrating the PFC and the DC-DC converter, a stacked structure will be used to ensure the unit fits within given volume restraints. This means that a support system will also need to be designed that can handle the anticipated loads while also keeping the weight of the entire RTRU under the 12 pound limit.

Appendix A Full Thermal Simulation Results

This appendix includes the results from all heat sink models at each of the three loading conditions analyzed throughout the course of this study. Every geometric parameter of each design is detailed along with the predicted pressure drop and predicted maximum device temperatures (assuming 25°C air at the inlet). The first number in the model name corresponds to the model number and the second corresponds to the loading condition. For example, "Model 096-150" means those are the results for Model number 96 at the 150 percent loading condition.

	Base Length (m)	Base Width (m)	Base Height (m)	Overall Height (m)	Fin Length (m)	No. Fins	Fin Width (m)	Heat Sink Weight (lbs)	Fin Spacing (m)	Pressure Drop (Pa)	Heat Sink Max Temp (°C)	MOSFET Max Temp (°C)	Diode Max Temp (°C)
Model 096-100	0.200	0.075	0.005	0.025	0.02	11	0.0025	1.10	0.00475	39	42	47	51
Model 096-150	0.200	0.075	0.005	0.025	0.02	11	0.0025	1.10	0.00475	39	52	61	64
Model 096-200	0.200	0.075	0.005	0.025	0.02	11	0.0025	1.10	0.00475	39	63	76	79
Model 108-100	0.200	0.075	0.005	0.03	0.025	11	0.0025	1.26	0.00475	44	39	45	48
Model 108-150	0.200	0.075	0.005	0.03	0.025	11	0.0025	1.26	0.00475	44	48	56	60
Model 108-200	0.200	0.075	0.005	0.03	0.025	11	0.0025	1.26	0.00475	44	57	70	74
Model 109-100	0.200	0.075	0.005	0.035	0.03	11	0.0025	1.43	0.00475	50	37	43	46
Model 109-150	0.200	0.075	0.005	0.035	0.03	11	0.0025	1.43	0.00475	50	44	53	57
Model 109-200	0.200	0.075	0.005	0.035	0.03	11	0.0025	1.43	0.00475	50	53	66	69
Model 098-100	0.200	0.075	0.005	0.04	0.035	11	0.0025	1.59	0.00475	70	36	41	44
Model 098-150	0.200	0.075	0.005	0.04	0.035	11	0.0025	1.59	0.00475	70	42	50	55
Model 098-200	0.200	0.075	0.005	0.04	0.035	11	0.0025	1.59	0.00475	70	49	62	66
Model 111-100	0.200	0.075	0.003	0.023	0.02	11	0.0025	0.92	0.00475	30	43	48	51
Model 111-150	0.200	0.075	0.003	0.023	0.02	11	0.0025	0.92	0.00475	30	53	62	66
Model 111-200	0.200	0.075	0.003	0.023	0.02	11	0.0025	0.92	0.00475	30	66	78	81

Table A-1: Thermal simulation results part 1 of 4

	Base Length (m)	Base Width (m)	Base Height (m)	Overall Height (m)	Fin Length (m)	No. Fins	Fin Width (m)	Heat Sink Weight (lbs)	Fin Spacing (m)	Pressure Drop (Pa)	Heat Sink Max Temp (°C)	MOSFET Max Temp (°C)	Diode Max Temp (°C)
Model 112-100	0.200	0.075	0.003	0.028	0.025	11	0.0025	1.09	0.00475	34	40	45	49
Model 112-150	0.200	0.075	0.003	0.028	0.025	11	0.0025	1.09	0.00475	34	49	58	62
Model 112-200	0.200	0.075	0.003	0.028	0.025	11	0.0025	1.09	0.00475	34	59	72	75
Model 114-100	0.200	0.075	0.003	0.033	0.03	11	0.0025	1.25	0.00475	40	38	43	47
Model 114-150	0.200	0.075	0.003	0.033	0.03	11	0.0025	1.25	0.00475	40	46	55	58
Model 114-200	0.200	0.075	0.003	0.033	0.03	11	0.0025	1.25	0.00475	40	55	68	71
Model 106-100	0.200	0.075	0.003	0.038	0.035	11	0.0025	1.41	0.00475	48	37	42	45
Model 106-150	0.200	0.075	0.003	0.038	0.035	11	0.0025	1.41	0.00475	48	43	52	56
Model 106-200	0.200	0.075	0.003	0.038	0.035	11	0.0025	1.41	0.00475	48	51	64	67
Model 110-100	0.200	0.075	0.003	0.04	0.037	11	0.0025	1.48	0.00475	62	36	41	45
Model 110-150	0.200	0.075	0.003	0.04	0.037	11	0.0025	1.48	0.00475	62	42	51	55
Model 110-200	0.200	0.075	0.003	0.04	0.037	11	0.0025	1.48	0.00475	62	50	62	66
Model 107-100	0.200	0.075	0.001	0.021	0.02	11	0.0025	0.74	0.00475	24	45	50	53
Model 107-150	0.200	0.075	0.001	0.021	0.02	11	0.0025	0.74	0.00475	24	57	65	68
Model 107-200	0.200	0.075	0.001	0.021	0.02	11	0.0025	0.74	0.00475	24	71	83	84
Model 113-100	0.200	0.075	0.001	0.026	0.025	11	0.0025	0.91	0.00475	28	42	47	50
Model 113-150	0.200	0.075	0.001	0.026	0.025	11	0.0025	0.91	0.00475	28	52	60	64
Model 113-200	0.200	0.075	0.001	0.026	0.025	11	0.0025	0.91	0.00475	28	64	76	77
Model 115-100	0.200	0.075	0.001	0.031	0.03	11	0.0025	1.07	0.00475	33	40	44	48
Model 115-150	0.200	0.075	0.001	0.031	0.03	11	0.0025	1.07	0.00475	33	48	57	60
Model 115-200	0.200	0.075	0.001	0.031	0.03	11	0.0025	1.07	0.00475	33	59	71	73
Model 116-100	0.200	0.075	0.001	0.036	0.035	11	0.0025	1.24	0.00475	40	38	43	46
Model 116-150	0.200	0.075	0.001	0.036	0.035	11	0.0025	1.24	0.00475	40	46	54	58
Model 116-200	0.200	0.075	0.001	0.036	0.035	11	0.0025	1.24	0.00475	40	55	67	69
Model 099-100	0.200	0.075	0.001	0.038	0.037	11	0.0025	1.30	0.00475	44	37	42	46
Model 099-150	0.200	0.075	0.001	0.038	0.037	11	0.0025	1.30	0.00475	44	44	53	57
Model 099-200	0.200	0.075	0.001	0.038	0.037	11	0.0025	1.30	0.00475	44	53	65	68
Model 105-100	0.200	0.075	0.001	0.04	0.039	11	0.0025	1.37	0.00475	55	37	41	46
Model 105-150	0.200	0.075	0.001	0.04	0.039	11	0.0025	1.37	0.00475	55	44	52	56
Model 105-200	0.200	0.075	0.001	0.04	0.039	11	0.0025	1.37	0.00475	55	52	64	67

Table A-2: Thermal simulation results part 2 of 4

	Base Length (m)	Base Width (m)	Base Height (m)	Overall Height (m)	Fin Length (m)	No. Fins	Fin Width (m)	Heat Sink Weight (lbs)	Fin Spacing (m)	Pressure Drop (Pa)	Heat Sink Max Temp (°C)	MOSFET Max Temp (°C)	Diode Max Temp (°C)
Model 128-100	0.200	0.075	0.005	0.04	0.035	11	0.002	1.36	0.00530	57	36	41	45
Model 128-150	0.200	0.075	0.005	0.04	0.035	11	0.002	1.36	0.00530	57	43	51	56
Model 128-200	0.200	0.075	0.005	0.04	0.035	11	0.002	1.36	0.00530	57	50	63	67
Model 129-100	0.200	0.075	0.005	0.04	0.035	11	0.0015	1.13	0.00585	48	37	42	46
Model 129-150	0.200	0.075	0.005	0.04	0.035	11	0.0015	1.13	0.00585	48	44	52	57
Model 129-200	0.200	0.075	0.005	0.04	0.035	11	0.0015	1.13	0.00585	48	52	65	68
Model 100-100	0.200	0.075	0.005	0.04	0.035	11	0.001	0.90	0.00640	39	38	43	46
Model 100-150	0.200	0.075	0.005	0.04	0.035	11	0.001	0.90	0.00640	39	45	53	58
Model 100-200	0.200	0.075	0.005	0.04	0.035	11	0.001	0.90	0.00640	39	53	66	70
Model 101-100	0.200	0.075	0.005	0.04	0.035	15	0.0015	1.38	0.00375	71	35	40	44
Model 101-150	0.200	0.075	0.005	0.04	0.035	15	0.0015	1.38	0.00375	71	40	49	53
Model 101-200	0.200	0.075	0.005	0.04	0.035	15	0.0015	1.38	0.00375	71	47	60	64
Model 130-100	0.200	0.075	0.005	0.04	0.035	15	0.001	1.07	0.00429	53	35	40	44
Model 130-150	0.200	0.075	0.005	0.04	0.035	15	0.001	1.07	0.00429	53	41	50	55
Model 130-200	0.200	0.075	0.005	0.04	0.035	15	0.001	1.07	0.00429	53	49	61	65
Model 135-100	0.200	0.075	0.005	0.04	0.035	15	0.0005	0.76	0.00482	43	37	42	46
Model 135-150	0.200	0.075	0.005	0.04	0.035	15	0.0005	0.76	0.00482	43	44	52	57
Model 135-200	0.200	0.075	0.005	0.04	0.035	15	0.0005	0.76	0.00482	43	52	64	68
Model 102-100	0.200	0.075	0.005	0.04	0.035	18	0.0015	1.57	0.00282	93	34	39	42
Model 102-150	0.200	0.075	0.005	0.04	0.035	18	0.0015	1.57	0.00282	93	39	47	51
Model 102-200	0.200	0.075	0.005	0.04	0.035	18	0.0015	1.57	0.00282	93	45	57	61
Model 131-100	0.200	0.075	0.005	0.04	0.035	18	0.001	1.20	0.00335	68	34	39	43
Model 131-150	0.200	0.075	0.005	0.04	0.035	18	0.001	1.20	0.00335	68	40	48	52
Model 131-200	0.200	0.075	0.005	0.04	0.035	18	0.001	1.20	0.00335	68	46	58	62
Model 133-100	0.200	0.075	0.005	0.04	0.035	18	0.0005	0.82	0.00388	52	36	41	44
Model 133-150	0.200	0.075	0.005	0.04	0.035	18	0.0005	0.82	0.00388	52	42	50	55
Model 133-200	0.200	0.075	0.005	0.04	0.035	18	0.0005	0.82	0.00388	52	49	62	65
Model 132-100	0.200	0.075	0.005	0.04	0.035	25	0.001	1.49	0.00208	117	33	38	42
Model 132-150	0.200	0.075	0.005	0.04	0.035	25	0.001	1.49	0.00208	117	38	46	50
Model 132-200	0.200	0.075	0.005	0.04	0.035	25	0.001	1.49	0.00208	117	43	56	60

Table A-3: Thermal simulation results part 3 of 4

	Base Length (m)	**Base Width (m)**	**Base Height (m)**	**Overall Height (m)**	**Fin Length (m)**	**No. Fins**	**Fin Width (m)**	**Heat Sink Weight (lbs)**	**Fin Spacing (m)**	**Pressure Drop (Pa)**	**Heat Sink Max Temp (°C)**	**MOSFET Max Temp (°C)**	**Diode Max Temp (°C)**
Model 134-100	0.200	0.075	0.005	0.04	0.035	25	0.0005	0.97	0.00260	76	34	39	43
Model 134-150	0.200	0.075	0.005	0.04	0.035	25	0.0005	0.97	0.00260	76	39	48	52
Model 134-200	0.200	0.075	0.005	0.04	0.035	25	0.0005	0.97	0.00260	76	45	58	62
Model 136-100	0.200	0.075	0.005	0.04	0.035	35	0.0005	1.18	0.00169	122	33	38	42
Model 136-150	0.200	0.075	0.005	0.04	0.035	35	0.0005	1.18	0.00169	122	38	46	50
Model 136-200	0.200	0.075	0.005	0.04	0.035	35	0.0005	1.18	0.00169	122	43	56	60
Model 139-100	0.200	0.075	0.005	0.04	0.035	45	0.0005	1.38	0.00119	186	33	38	42
Model 139-150	0.200	0.075	0.005	0.04	0.035	45	0.0005	1.38	0.00119	186	38	46	50
Model 139-200	0.200	0.075	0.005	0.04	0.035	45	0.0005	1.38	0.00119	186	43	56	59
Model 143-100	0.200	0.075	0.005	0.04	0.035	50	0.0005	1.49	0.00102	209	33	38	42
Model 143-150	0.200	0.075	0.005	0.04	0.035	50	0.0005	1.49	0.00102	209	38	46	50
Model 143-200	0.200	0.075	0.005	0.04	0.035	50	0.0005	1.49	0.00102	209	43	56	60

Table A-4: Thermal simulation results part 4 of 4

Appendix B Performance Plots for 100% and 150% Loads

This appendix includes the performance plots discussed in section 3.4.2 but for the 100% and 150% loading conditions. The shapes of these plots are the same as those presented in section 3.4.2 but the device temperatures vary.

B.1 Base Height and Fin Length Study Results

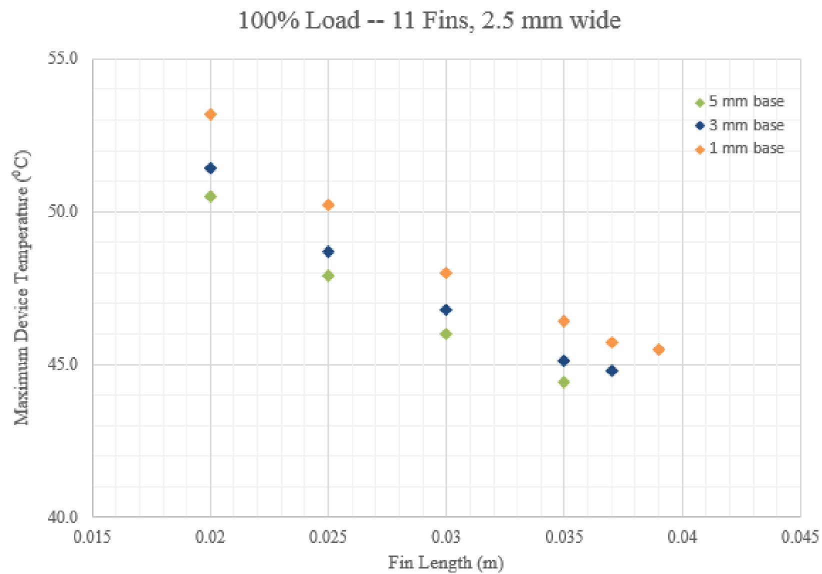

Figure B-1: Base Height and Fin Length Study Results - 100% Load

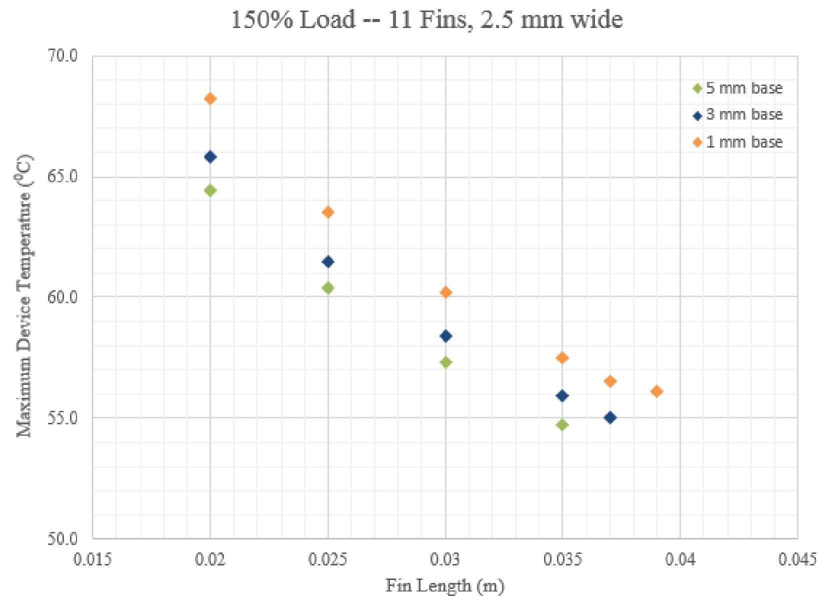

Figure B-2: Base Height and Fin Length Study Results - 150% Load

B.2 Fin Width and Number of Fins Study Results

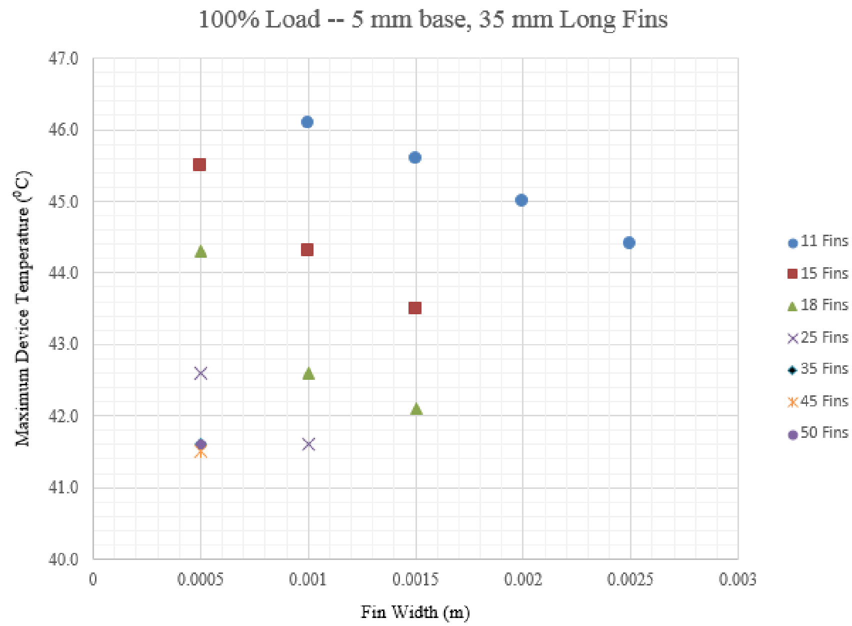

Figure B-3: Fin Width and Number of Fins Study - 100% Load

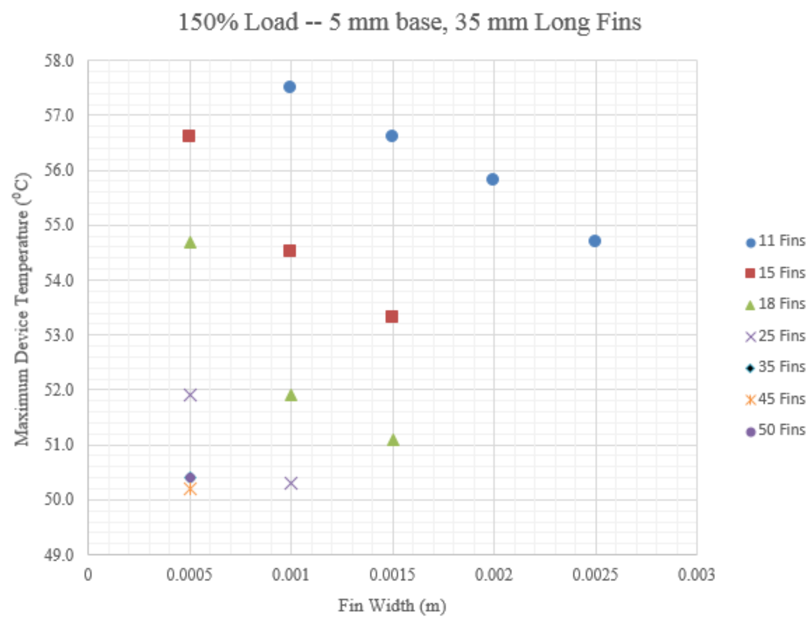

Figure B-4: Fin Width and Number of Fins Study - 150% Load

References

[1] McCluskey, F. Patrick, Thomas Podlesak, and Richard Grzybowski. *High Temperature Electronics*. CRC press, 1996.

[2] Colgan, Evan G., Bruce Furman, Michael Gaynes, Willian S. Graham, Nancy C. LaBianca, John H. Magerlein, Robert J. Polastre et al. "A practical implementation of silicon microchannel coolers for high power chips." *Components and Packaging Technologies, IEEE Transactions on* 30, no. 2 (2007): 218-225.

[3] Sakanova, Assel, Chin Fong Tong, Arie Nawawi, Rejeki Simanjorang, K. J. Tseng, and A. K. Gupta. "Investigation on weight consideration of liquid coolant system for power electronics converter in future aircraft." *Applied Thermal Engineering* 104 (2016): 603-615.

[4] Bergman, Theodore L., Frank P. Incropera, and Adrienne S. Lavine. *Fundamentals of Heat and Mass Transfer*. John Wiley & Sons, 2011.

[5] Kraus, Allan D., and Avram Bar-Cohen. *Design and Analysis of Heat Sinks*. New York: Wiley, 1995.

[6] "Cree CMF10120D Silicon Carbide Power MOSFET datasheet." *Cree Inc.* http://www.mouser.com/ds/2/90/CMF10120D-276049.pdf. Accessed March 23, 2016.

[7] "Cree C2D05120A Silicon Carbide Schottky Diode datasheet." *Cree Inc.* http://www.datasheetspdf.com/PDF/C2D05120/561195/1. Accessed March 23, 2016.

[8] "Cree CPW2-0600-S010B Silicon Carbide Schottky Diode Chip datasheet." *Wolfspeed.* http://www.wolfspeed.com/power/products/sic-schottky-diodes/table. Accessed March 23, 2016.

[9] "Cree CPM2-1200-0080B Silicon Carbide Power MOSFET Chip datasheet." *Wolfspeed.* http://www.wolfspeed.com/power/products/sic-mosfets/table. Accessed March 23, 2016.

[10] Sauciuc, Ioan, Greg Chrysler, Ravi Mahajan, and Michele Szleper. "Air-Cooling Extension-Performance Limits for Processor Cooling Applications." In *Semiconductor Thermal Measurement and Management Symposium, 2003. Ninteenth Annual IEEE*, pp. 74-81. IEEE, 2003.

[11] "Transformer Rectifier Units." *Crane Aerospace and Electronics.* Accessed June 9, 2016. http://www.craneae.com/Products/Power/TransformerRectifierUnit.aspx

[12] "AC-DC Transformer Rectifier Units." *Avionics Instruments LLC.* Accessed June 10, 2016. http://www.avionicinstruments.com/transformer-rectifier-units

[13] Lasance, Clemens JM. "Heat Spreading: Not a Trivial Problem." *Electronics Cooling* 14, no. 2 (2008): 24.

[14] Lee, Seri. "Calculating Spreading Resistance in Heat Sinks." *Electronics Cooling* 4 (1998): 30-33.

[15] Behnia, Masud, David Copeland, and Denpong Soodphakdee. "A Comparison of Heat Sink Geometries for Laminar Forced Convection: Numerical Simulation of Periodically Developed Flow." In *Thermal and Thermomechanical Phenomena in Electronic Systems, 1998. ITHERM'98. The Sixth Intersociety Conference on*, pp. 310-315. IEEE, 1998.

[16] Kim, Sung Jin, Dong-Kwon Kim, and Hwan Hee Oh. "Comparison of Fluid Flow and Thermal Characteristics of Plate-Fin and Pin-Fin Heat Sinks Subject to a Parallel Flow." *Heat Transfer Engineering* 29, no. 2 (2008): 169-177.

[17] Lee, Seri. "Optimum Design and Selection of Heat Sinks." In *Semiconductor Thermal Measurement and Management Symposium, 1995. SEMI-THERM XI., Eleventh Annual IEEE*, pp. 48-54. IEEE, 1995.

[18] Krueger, William B., and Avram Bar-Cohen. "Optimal Numerical Design of Forced Convection Heat Sinks." *Components and Packaging Technologies, IEEE Transactions on* 27, no. 2 (2004): 417-425.

[19] Iyengar, M., and A. Bar-Cohen. "Design for Manufacturability of Forced Convection Air Cooled Fully Ducted Heat Sinks." *Electronics Cooling* 13, no. 3 (2007): 12.

[20] Iyengar, Madhusudan, and Avram Bar-Cohen. "Design for Manufacturability of SISE Parallel Plate Forced Convection Heat Sinks." In *Thermal and Thermomechanical Phenomena in Electronic Systems, 2000. ITHERM 2000. The Seventh Intersociety Conference on*, vol. 1. IEEE, 2000.

[21] Icepak, A. N. S. Y. S. "12.0 User's Guide." *Fluent Inc.* (2009).

[22] "Therm-A-Gap Thermally Conductive Gap Filler Pads." *Chomerics – Parker Division*. Accessed April 26, 2016. http://vendor.parker.com/852568C80043FA7A/468ea5de5ac341d385257d39005641c7/586CF13E3B4B8FF08525729600612C6C/$FILE/THERM-A-GAP_500_Series_TB-1016-1-07.pdf

[23] Tuckerman, David B., and R. F. W. Pease. "High-Performance Heat Sinking for VLSI." *Electron Device Letters, IEEE* 2, no. 5 (1981): 126-129.

[24] MSC Industrial Supply Co. Accessed April 5, 2016. http://www.mscdirect.com/browse/tn/Milling/Milling-Saws/SlittingSlotting-Saws?navid=12106272.

[25] "AFC0912DE-7X60 Delta DC Brushless Axial Fan Specification Sheet." *Delta Electronics Component Company*. Issued January 22, 2008. Accessed April 20, 2016. http://www1.futureelectronics.com/doc/DELTA%20PRODUCTS%20CORPORATION/AFC0912DE-7X60.pdf

[26] Stevens, Mark. "Fan Performance." *Air Movement and Control Association International.* Accessed April 20, 2016. https://www.amca.org/UserFiles/file/Mark%20paper.pdf

[27] "Minimizing System Effect." *The News.* Published July 22, 2005. Accessed April 21, 2016. http://www.achrnews.com/articles/96369-minimizing-system-effect

[28] Candan, Zeki, Umit Büyüksarı, Süleyman Korkut, Oner Unsal, and Nevzat Çakıcıer. "Wettability and surface roughness of thermally modified plywood panels." *Industrial Crops and Products* 36, no. 1 (2012): 434-436.